A double scale fast algorithm for the transient evolution of a resonant tunneling diode

Naoufel Ben Abdallah, Ali Faraj

Finite difference and double scale fast algorithm for time-dependent quantum resonant transport

N. Ben Abdallah*, A. Faraj†

Abstract

The simulation of the time-dependent evolution of the resonant tunneling diode is done by a multiscale algorithm exploiting the existence of resonant states. After revisiting the algorithm developed in [N. Ben Abdallah, O. Pinaud, J. Comput. Phys. 213, 1 (2006) 288-310] for the stationary case, the time-dependent problem is dealt with. The wave function is decomposed into a non resonant part and a resonant one. The projection method to compute the resonant part leads to an accurate algorithm thanks to a suitable interpolation of the non resonant one. The simulation times are largely reduced.

Keywords: Schrödinger equation; numerical scheme; resonant tunneling diode; resonant states; time-dependent.

Subject classifications: 35Q41, 35Q55, 65M99, 65Z05, 81-08, 81V99

1 Introduction

The Resonant Tunneling Diode (RTD) is a heterostructure made of a superposition of thin layers of semiconductor of different types used to create double or multiple potential barriers. The possibility of resonant tunneling through multiple barriers and the resulting negative differential resistance were firstly discussed in [30, 42]. Such physical effects make the RTD useful in the conception of signal generators, detectors and mixers, multi-valued logic switches, low-power amplifiers, local oscillators, frequency locking circuits, and also as generators of multiple high frequency harmonics, see [33].

In the mathematical and numerical models for the RTD, it is natural to incorporate the quantum effects described above. In particular, due to the small size of the device, the kinetic models for semi-conductors [24, 39] have to be replaced by their natural extension to the quantum level: the Wigner equation or equivalently a system of infinitely many Schrödinger equations. In the last models, the electron interaction can represented thanks to a Poisson equation, which leads to the Wigner-Poisson [16, 32] or Schrödinger-Poisson system [6, 7, 35]. Both approaches are able to recover the negative differential resistance in the I-V characteristics, however, it was shown in [29, 40] that the second approach could lead to hysteresis phenomena in agreement with physical observations.

For the Schrödinger-Poisson system, which will be adopted in the present work, the nonlinear coupling effects take place in the middle of the structure. This active region is out of equilibrium and connected to the exterior through access zones which allow the injection of electrons. Therefore, a first important issue is to find suitable transparent boundary conditions for the Schrödinger equation at the boundary of the active region. Such boundary conditions have been derived and analyzed in [2, 6, 7, 22] and in [3, 18, 31] for the discrete solution involved in the simulations.

Other theoretical studies were devoted to the Schrödinger-Poisson system, dealing with the well-posedness of the nonlinear problem [6, 7, 35] and the derivation of asymptotic models [14, 15, 29, 40]

*Université de Toulouse, Institut de Mathématiques de Toulouse, UMR - CNRS 5219, Université Paul Sabatier, 31062 Toulouse Cedex 9, France

†Grenoble INP - ESISAR, 50 rue Barthélémy de Laffemas BP 54 - 26902 Valence Cedex 9 - France

for the RTD. The last summarize how a finite number of resonant states may produce several nonlinear solutions. In the stationary case, the authors in [13] used such a simplified model to perform fast simulations of the RTD and obtained in [12] at least a quantitative agreement with the complete model numerical solution.
The simulation of the RTD is a challenging problem due to the presence of quantum resonances which create stiff variations of the wave function with respect to the frequency variable and increase dramatically the numerical complexity. In that context, the reduction of the simulation time provided by the simplified models described above is of particular interest. Nevertheless, more accurate fast simulations were obtained in the stationary case in [8] by working on the complete Schrödinger-Poisson system. In [8], in addition to a new WKB finite element method (see also [5, 34]), the reduction of the simulation time is provided by an adapted treatment of the transmission peaks using resonant modes. In the time-dependent case, the supplementary numerical cost imposed by resonances is even more important and its reduction even more challenging. Indeed, the numerical complexity of the transparent boundary conditions of each time-dependent Schrödinger equation is of order one with respect to the number of time iterations which is necessarily big since the period of the injected free plane waves with higher energy is much smaller than the scaling time of the system. Moreover, although advances (based on the adiabatic theorem) has been made in [20, 21] in order to extend the simplified model simulations in [12, 13] to the time-dependent regime, no fast accurate algorithm similar to [8] was proposed for the resolution of the RTD transient Schrödinger-Poisson system. This is the aim of the present work.
In our RTD model, the classical observables, like electronic and current densities, are given by integrals on the frequency variable involving the wave function. To compute correctly these integrals, a uniform frequency mesh has to be very thin to be able to capture the resonance peaks. The high number of Schrödinger equations to be solved, and therefore the high numerical cost, of this standard approach was reduced in the stationary regime in [38] using adaptive refinement. The last method does however not extend to the transient case since the resonant frequencies do move as time varies. Lately, inspired by an idea from [40], the algorithm in [8] was proposed for the discretization of the stationary system. The method consists in decomposing the wave function in a resonant part living between the double barrier and a non resonant part which is mostly localized outside this well. The non resonant part is smooth with respect to the frequency variable whereas the resonant one has sharp peaks at resonant frequencies. The latter is computed by a projection method after a precomputation of resonant states. Due to the sharpness of the resonance peaks, this process can not succeed without an accurate value of resonance energies and widths. Therefore, we first present an improvement of the method used in [8] to compute these values. The problem of finding quantum resonances has interested many authors, e.g. [11, 41]. As it is done in [19, 36], the one dimensional problem can be written as a differential equation with homogeneous transparent boundary conditions selecting outgoing functions. Starting from this approach, we write the problem of finding resonances at the discrete level. Since the spectral parameter is involved nonlinearly in the boundary conditions, this discrete problem is a nonlinear eigenvalue problem. To solve the nonlinear eigenvalue problem, we derive a Newton-like method which extends to holomorphic matrices the method proposed in [37] for polynomials. Additional references concerning the resolution of nonlinear eigenvalue problems can be found in [25].
We remark that in the present case, the Fermi-Dirac distribution involved in the densities operates like a frequency cutoff and only the first mode is important in the above resonant part. The multi-mode approximation follows the same line and finds applications in the simulation of the stationary two-dimensional RTD, see [9].
Thereafter, we give our fast transient double scale algorithm which adapts and extends to the time-dependent case the algorithm of [8]. As in the stationary regime, the algorithm consists in decomposing the wave function in a resonant part and a non resonant one. For the latter, the frequency mesh can be chosen coarse enough thus reducing the number of Schrödinger equations to be solved and the simulation time. For the former, a single spatial problem (the computation of the resonant mode) is solved for all the frequency points. Therefore a refined frequency mesh can be used for the projection on the resonant mode, capturing this way the resonant peak without increasing significantly the numerical cost. Due to the scale difference between the two parts, the

projection method requires an interpolation of the non resonant one and the algorithm is accurate only if this interpolation takes into account the time oscillations coming from the Schrödinger equation.
The method we use for the numerical resolution of the time-dependent Schrödinger equation corresponds to a suitable adaptation to the nonlinear case of the Crank-Nicolson finite difference scheme along with the transparent boundary conditions in [3, 18]. Our scheme is provided by the extrapolation of the intermediary potential in [17] which corresponds to a modified Adams-Bashforth-Crank-Nicolson method. We show that such an extrapolation allows bigger time steps than the extrapolation in [38] which is also considered in [10] for a different kind of nonlinearity. In the stationary case, the nonlinearity of the Schrödinger-Poisson system is dealt with using the self-consistent scheme in [38], see also [26].
The boundary conditions in [3, 18] are adopted here since they have the advantage to be verified exactly by the whole space discrete solution. We note that they can be used to write several kind of finite difference schemes, including splitting methods, to solve time-dependent nonlinear Schrödinger equations, see [43]. In the different L^2 context, the numerical resolution of the time-dependent nonlinear Schrödinger equation has been investigated by many authors, e.g. [4, 28] and, in the case of the bounded domain, [17]. Applying additional results from [3, 18] to our RTD model, we verify numerically that, compared to the results in [38], the transparent boundary conditions for the Schrödinger equation can be simplified to reduce the computational time and fitted, without increasing the computational time, to improve the accuracy.
In order to be able to compare the time-dependent solution to the stationary one in a meaningful manner, the discretization of the space variable must be the same for the two regimes. Therefore, we will employ a standard finite difference method along with the stationary boundary conditions in [3] to solve the stationary Schrödinger equation and concentrate on the frequency variable to handle the resonance peaks. Similarly, in the wave function decomposition performed in our new fast algorithm, the resonant part is computed using finite difference in order to be consistent with the non resonant one. For that purpose, we give a definition of a resonance in the sense of the finite difference discrete Schrödinger equation and write the discrete boundary conditions for the corresponding resonant mode. The last are extensions to complex valued energies of a homogeneous version of the stationary boundary conditions. These boundary conditions are verified exactly by the resonant mode thanks to the following strategy: first we considered the discretization of the differential equation on the whole space, and then we derived the boundary conditions for the difference scheme directly on a purely discrete level.
The paper is organized as follows. In section 2, are presented the stationary and time-dependent Schrödinger-Poisson systems. The stationary case is dealt with in section 3 where are given the reference method, the adaptive refinement method and two methods based on the projection on the resonant mode. Our method to compute resonances and resonant modes is also introduced. In section 4, the time-dependent reference method is recalled and our improved transient algorithm is presented. The numerical results are given in section 5. The different methods are compared in the stationary and in the time-dependent case. In the time-dependent case, the comparison shows the improvement provided by our new algorithm and the existence of two resonant peaks is verified. In the appendix are given the finite difference methods with discrete transparent boundary conditions to solve the stationary and time-dependent Schrödinger equation. For the time-dependent scheme, the Schrödinger equation is supposed to be linear and a stability result is proven in the situation of the continuous influx in the device. The discrete problem for the computation of resonances is also obtained and the properties of the solution are studied.

2 The model

The model consists in an infinite number of Schrödinger equations coupled to the Poisson equation. The Schrödinger equation involves the time-dependent Hamiltonian

$$H(t) = -\frac{\hbar^2}{2m}\partial_x^2 + U(t) + V(t),$$

where $\hbar$ is the reduced Planck constant, m is the effective mass of the electron and $x \in \mathbb{R}$ is the position variable. The domain occupied by the device is the interval $[0, L]$, $L > 0$. The external potential $U(t)$ describes the double barrier and the applied bias, see Figure 1, and is given as if a data of the problem. Given the points

$$0 < a_1 < a_2 < a_3 < b_3 < b_2 < b_1 < L\,,$$

the external potential writes

$$U(t) = v_0 \mathbf{1}_{[a_2,a_3[\cup]b_3,b_2]} - B(t)\Big(\frac{x-a_1}{b_1-a_1}\mathbf{1}_{[a_1,b_1[} + \mathbf{1}_{[b_1,+\infty[}\Big)\,,$$

where $v_0 \geq 0$ and $B(t) \geq 0$ are scalars representing respectively the height of the barrier and the amplitude of the applied bias. The points a_1 and b_1 are the extremities of the diode. The interval $[a_3, b_3]$ is the quantum well. The problem is the following infinite system of Schrödinger equations

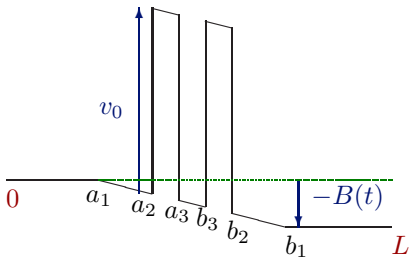

Figure 1: External potential $U(t)$.

$$\begin{cases} i\hbar\partial_t \Psi_k(t) = -\frac{\hbar^2}{2m}\partial_x^2 \Psi_k(t) + (U(t) + V(t))\Psi_k(t), \quad x \in \mathbb{R} \\ \Psi_k(0) = \Phi_k \end{cases} \tag{2.1}$$

where the initial condition Φ_k, defined at the end of this section, is a generalized eigenfunction of the initial Hamiltonian $H(0)$ corresponding to the frequency $k \in \mathbb{R}$. The self-consistent potential $V(t)$, which is due to Coulomb interaction, depends nonlinearly on the wave functions. It satisfies the Poisson equation:

$$\begin{cases} -\partial_x^2 V(t) = \frac{q^2}{\varepsilon}(n(t) - n_D), \quad (0, L) \\ V(t, 0) = V(t, L) = 0, \end{cases} \tag{2.2}$$

and is extended by 0 outside $(0, L)$. In (2.2), q is the elementary charge of the electron, ε is the dielectric constant, n_D is the doping equal to

$$n_D = n_D^1(\mathbf{1}_{[0,a_1[} + \mathbf{1}_{]b_1,L]}) + n_D^2 \mathbf{1}_{[a_1,b_1]},$$

with $n_D^1 > n_D^2 \geq 0$. The electron density $n(t)$ is given by:

$$n(t, x) = \int_{\mathbb{R}} g(k)|\Psi_k(t, x)|^2 dk\,. \tag{2.3}$$

In our model, the injection profile g is the one dimensional Fermi-Dirac distribution:

$$g(k) = \frac{mk_BT}{2\pi^2\hbar^2} \ln\left(1 + \exp\left(\frac{E_F - \frac{\hbar^2k^2}{2m}}{k_BT}\right)\right), \tag{2.4}$$

where k_B is the Boltzmann constant, T is the temperature of the semiconductor and E_F is the Fermi level.

In the stationary regime, the external potential is the potential $U_I = U(0)$ corresponding to the initial bias $B_I = B(0)$. The time-independent problem is the following infinite system of equations

$$-\frac{\hbar^2}{2m}\partial_x^2\Phi_k + (U_I + V_I)\Phi_k = E_k\Phi_k, \quad x \in I\!R, \tag{2.5}$$

with scattering conditions

$$\begin{cases} \Phi_k(x) = e^{ikx} + r(k)e^{-ikx}, & x < 0 \\ \Phi_k(x) = t(k)e^{i\sqrt{k^2+2mB_I/\hbar^2}x}, & x > L, \end{cases} \quad \text{for } k \geq 0 \tag{2.6}$$

and

$$\begin{cases} \Phi_k(x) = t(k)e^{-i\sqrt{k^2-2mB_I/\hbar^2}x}, & x < 0 \\ \Phi_k(x) = e^{ikx} + r(k)e^{-ikx}, & x > L, \end{cases} \quad \text{for } k < 0\,, \tag{2.7}$$

where

$$E_k = \begin{cases} \frac{\hbar^2k^2}{2m}, & k \geq 0 \\ \frac{\hbar^2k^2}{2m} - B_I, & k < 0\,. \end{cases} \tag{2.8}$$

As in the time-dependent case, the self-consistent potential V_I satisfies the Poisson equation:

$$\begin{cases} -\partial_x^2 V_I = \frac{q^2}{\varepsilon}(n_I - n_D), & (0, L) \\ V_I(0) = V_I(L) = 0, \end{cases} \tag{2.9}$$

and is extended by 0 outside $(0, L)$. The electron density n_I is given by:

$$n_I(x) = \int_{I\!R} g(k)|\Phi_k(x)|^2 dk\,. \tag{2.10}$$

3 The stationary algorithm revisited

3.1 Recalling the standard algorithm

To solve the stationary nonlinear Schrödinger-Poisson system (2.5)(2.9)(2.10), we will use the same algorithm as in [38]. It is based on a Gummel iteration, see [26], which consists in the computation of a sequence V_I^l, $l \geq 0$ where the potential V_I^{l+1} at step $l+1$ is deduced form the potential V_I^l at step l by solving the following nonlinear equation:

$$\begin{cases} -\partial_x^2 V_I^{l+1} = \frac{q^2}{\varepsilon}(n_I^l \exp((V_I^l - V_I^{l+1})/V_{ref}) - n_D), & (0, L) \\ V_I^{l+1}(0) = V_I^{l+1}(L) = 0\,, \end{cases} \tag{3.1}$$

for a fixed reference potential V_{ref}. In (3.1), n_I^l is the density (2.10) where the wave functions are solution to (2.5) with $V_I = V_I^l$.
The repartition function g being exponentially decreasing at infinity, the integral in (2.10) can be restricted, in computations, to a domain $[-\kappa, \kappa]$ where κ is chosen to be big enough. We consider a discretization $x_0 = 0, x_1, ..., x_j, ..., x_J = L$ of the interval $[0, L]$ with uniform grid spacing Δx and a discretization $k_0 = -\kappa, k_1, ..., k_p, ..., k_P = \kappa$ of the interval $[-\kappa, \kappa]$ with non-necessarily uniform grid spacing $\Delta k_p = k_{p+1} - k_p$. In order to verify, the condition (A.4) for all $k \in [-\kappa, \kappa]$, the grid spacing for the space variable is chosen such that:

$$\Delta x < \frac{1}{\sqrt{\kappa^2 + \frac{2m}{\hbar^2}B_I}}\,. \tag{3.2}$$

Then, for a given initial potential V_I^0, the algorithm writes:

Algorithm 3.1 (Gummel algorithm)**.**

Fix $l = 0$.
Set $\Delta = \text{tol} + 1$.
Do While $\Delta \geq \text{tol}$:

Computation of the density

$S1$. For $p = 0, ..., P$: computation of the wave function Φ_p^l at the frequency k_p from the potential V_I^l by solving equation (2.5) with $V_I = V_I^l$.

$S2$. Numerical integration: for $j = 0, ..., J$

$$n_{I,j}^l = \sum_{p=0}^{P-1} \left(g(k_p) \left| \Phi_{p,j}^l \right|^2 + g(k_{p+1}) \left| \Phi_{p+1,j}^l \right|^2 \right) \frac{\Delta k_p}{2}. \tag{3.3}$$

Coupling to the Poisson equation : Gummel iteration
Computation of the potential V_I^{l+1} from the potential V_I^l and the density n_I^l by solving equation (3.1).

Set

$$\Delta = \frac{\left| V_I^{l+1} - V_I^l \right|_2}{\left| V_I^{l+1} \right|_2}. \tag{3.4}$$

Set $l = l + 1$.
End Do.

In equation (3.3), $n_{I,j}^l$ denotes the approximation of the density $n_I^l(x_j)$ and $\Phi_{p,j}^l$ the approximation of the wave function $\Phi_p^l(x_j)$. In equation (3.4) and in what follows, $|v|_2$ denotes the l^2-norm of the vector $v \in \mathbb{C}^{J+1}$. Equation (3.1) is nonlinear and is solved with a Newton method where the Laplacian is discretized using finite difference at the points $(x_j)_{0 \leq j \leq J}$.
Because of the peaked form of the transmission near resonances, the method used to compute the density n_I^l from the potential V_I^l (steps $S1$ and $S2$) is of major importance, and the Gummel algorithm may fail to converge if a non accurate method is used.
In [38], the step $S1$ is performed without particular treatment of resonances: the function Φ_p^l is computed on $[0, L]$ by the resolution of the problem (2.5)-(2.8) with the finite difference scheme (A.3) and the discrete transparent boundary conditions (A.7), (A.10) for $k \geq 0$ and (A.11), (A.12) for $k < 0$ where the potential Q_I is replaced by $U_I + V_I^l$. In that case, the convergence is provided by the choice of the frequency mesh $\{k_p,\, p = 0, ..., P\}$ for the trapezoidal rule in the step $S2$. The reference method is obtained by taking the grid spacing Δk_p equal to a constant $\Delta k > 0$ small enough. This method will be called Direct Resolution. In order to reduce the high numerical cost, which is due to the big number of Schrödinger equations to be solved, an Adaptive Method is proposed in [38]. For the Adaptive Method, the grid spacing Δk_p is taken equal to the small constant Δk only when E_{k_p} is close to a resonant energy, otherwise $\Delta k_p = \nu \Delta k$ where $\nu \geq 2$. The frequency points where the mesh is refined are detected using the logarithmic derivative, with respect to the frequency k, of the transmission coefficient related to the wave function Φ_k (see [38, 19]).
As noticed in the introduction, the Adaptive Method can not be generalized to the time-dependent case. In this context, the One Mode Approximation algorithm presented in section 3.3 is very useful. As proposed in [8], this algorithm consists in decomposing the wave function in a non resonant part and a resonant part proportional to the first resonant mode. In [8], using a WKB interpolation to compute each part of the wave function, an adapted treatment of the step $S1$ is realized.
In the present work, we do not use the WKB interpolation, however the accuracy required at step $S1$ is reached by an improvement of the computation of the first resonance. In particular, a precise computation of its imaginary part is essential. A simple reconstitution of the wave functions not allowing to modify the frequency mesh, the gain in computational time is reached by adapting the

step $S2$. The first method proposed in the present work is inspired from [8]. It consists in using different frequency scales for the different parts of the wave function. The frequency mesh is taken thin only for the coefficient of proportionality to the resonant mode and the number of Schrödinger equations to be solved is reduced. This method will be denoted One Mode Approximation and will be generalized to the time-dependent case. A variant of this method is obtained by an explicit integration of the coefficient of proportionality to the resonant mode instead of the trapezoidal rule. In that case all the resonant peak is integrated and the frequency mesh can be chosen coarse enough. This method will be denoted One Mode Approximation Integ.
The algorithms Direct Resolution, Adaptive Method, One Mode Approximation and One Mode Approximation Integ are compared in section 5.2.

3.2 Accurate computation of resonances

In the founder work [1], see also [27], resonances of a self-adjoint operator are defined using analytic transformations, and it is a common fact that it corresponds to an eigenvalue in a modified L^2 space [23]. Adapting the second approach to potentials Q verifying

$$Q(x) = 0,\, x \leq 0 \quad \text{and} \quad Q(x) = Q_L,\, x \geq L \quad \text{where} \quad Q_L \leq 0 \tag{3.5}$$

a definition of the resonances of the Hamiltonian

$$-\frac{\hbar^2}{2m}\partial_x^2 + Q \tag{3.6}$$

is given in [36] and [19]. Starting from this definition, the resonances of the Hamiltonian (3.6) can be characterized as the numbers z in $\mathbb{C} \setminus \{i\mathbb{R} \cup i\mathbb{R} + Q_L\}$ such that the problem

$$\begin{cases} [-\frac{\hbar^2}{2m}\partial_x^2 + Q]u = zu, \quad \mathbb{R} \\ ||u||_{L^2(0,L)} = 1 \end{cases} \tag{3.7}$$

has solutions which are purely outgoing outside the interval $[0, L]$. The function u in (3.7) is called resonant mode associated to the resonance z. As described in Appendix B, the eigenproblem (3.7) is restricted (for numerical computations) to the domain $[0, L]$ by the aid of transparent boundary conditions selecting only outgoing states. In particular, this problem is discretized using the finite difference scheme (B.1) inside the domain and the boundary conditions (B.5), (B.8) at $x = 0$ and $x = L$. Since the boundary conditions depend nonlinearly on the spectral parameter z, this process leads to the following nonlinear eigenvalue problem: find $(u, z) \in \mathbb{C}^{J+1} \times \mathbb{C}$ such that

$$\begin{cases} M(z)u = 0 \\ u^H u = 1, \end{cases} \tag{3.8}$$

where $M(z)$ is the nonlinear matrix valued function of z given by (B.10) and u^H denotes the complex conjugate transpose of the vector u. A Newton-like method is introduced in [37] to solve (3.8) when $M(z)$ is a polynomial. Following the same line, we derive a method for the general case where $M(z)$ is holomorphic. Note first that the term $u^H u$ appearing in (3.8) is not differentiable with respect to u, therefore a Newton method must be modified to be applied here. For a given iterate (u^n, z^n) verifying $(u^n)^H u^n = 1$, we are looking for a direction $(\delta u^n, \delta z^n)$ such that $(u^n + \delta u^n, z^n + \delta z^n)$ is solution to problem (3.8). Using $(u^n)^H u^n = 1$ the system:

$$\begin{cases} M(z^n + \delta z^n)(u^n + \delta u^n) = 0 \\ (u^n + \delta u^n)^H (u^n + \delta u^n) = 1 \end{cases}$$

gives at order 2:

$$\begin{aligned} M(z^n)\delta u^n + \delta z^n M'(z^n)u^n &= -M(z^n)u^n, \\ (u^n)^H \delta u^n + (\delta u^n)^H u^n &= 0. \end{aligned} \tag{3.9}$$

As noticed earlier, there is a problem with the second equation, however, it is enough to impose $(u^n)^H \delta u^n = 0$ in order to verify (3.9). Therefore, we obtain the following linear system:

$$\begin{bmatrix} M(z^n) & M'(z^n)u^n \\ (u^n)^H & 0 \end{bmatrix} \begin{bmatrix} \delta u^n \\ \delta z^n \end{bmatrix} = \begin{bmatrix} -r^n \\ 0 \end{bmatrix}, \quad \text{where } r^n = M(z^n)u^n. \tag{3.10}$$

Its resolution corresponds to an iteration of our Newton-like method to compute the resonant mode and the resonance. The assumption $(u^n)^H u^n = 1$ we made to obtain the system (3.10) is verified at order 2 as long as $(u^0)^H u^0 = 1$.

3.3 The One Mode Approximation

We start with the description of the step $S1$, in the One Mode Approximation, of the computation of a wave function Φ_k solution to the stationary Schrödinger equation (2.5) for a given frequency k. The exponent l appearing in Algorithm 3.1 is omitted in order to simplify notations. Following the works [8] and [40], the One Mode Approximation consists in the decomposition:

$$\Phi_k = \Phi_k^{nr} + \Phi_k^r \,, \tag{3.11}$$

where the non resonant part Φ_k^{nr} solves the stationary Schrödinger equation:

$$[-\frac{\hbar^2}{2m}\partial_x^2 + U_{I,fill} + V_I]\Phi_k^{nr} = E_k \Phi_k^{nr}, \quad x \in I\!R \,, \tag{3.12}$$

with filled potential $U_{I,fill} = U_I + v_0 \mathbf{1}_{[a_3,b_3]}$. Equation (3.12) comes with the scattering conditions (2.6), (2.7) and the relation (2.8). It is solved on $[0, L]$ using the finite difference scheme (A.3) and the discrete transparent boundary conditions (A.7), (A.10) for $k \geq 0$ and (A.11), (A.12) for $k < 0$ where the potential Q_I is replaced by $U_{I,fill} + V_I$. The statistic g being rapidly decreasing at infinity, the resonant part Φ_k^r is searched, on $[0, L]$, proportional to the resonant mode u_I of minimal resonant energy $\mathrm{Re}\,(z_I)$ verifying

$$[-\frac{\hbar^2}{2m}\partial_x^2 + U_I + V_I]u_I = z_I u_I \tag{3.13}$$

and $\int_0^L |u_I(x)|^2 dx = 1$. In other words, we look for Φ_k^r of the form:

$$\Phi_k^r(x) = \theta_k u_I(x), \quad x \in [0, L] \,. \tag{3.14}$$

Like in [8], the condition that Φ_k verifies the stationary Schrödinger equation (2.5) gives the following explicit value of the proportionality coefficient:

$$\theta_k = \frac{1}{z_I - E_k} v_0 \int_{a_3}^{b_3} \Phi_k^{nr} \overline{u_I} dx. \tag{3.15}$$

The resonant mode and the resonance are computed using the method presented in section 3.2 with the potential $Q = U_I + V_I$. This method is initialized at the fundamental mode and fundamental energy, (u_D, E_D), of the Hamiltonian

$$[-\frac{\hbar^2}{2m}\partial_x^2 + U_I + V_I] \tag{3.16}$$

equipped with homogeneous Dirichlet boundary conditions at a_2 and b_2. It's shown in [14][15] that the real part of resonances are well approached by the eigenvalues of the Dirichlet Hamiltonian (3.16). The imaginary part of resonances being small, such an initialization insures the convergence of the algorithm to the resonance with smaller energy. This achieves the step $S1$.
For the One Mode Approximation, the step $S2$ consists in using the wave function decomposition in order to compute accurately the density with a low numerical cost. First, using an argument of

localization of support, see [40], the cross term in the development of $|(\Phi_k^{nr} + \theta_k u_I)(x)|^2$ can be neglected, which gives the approximation:

$$n_I(x) = \int_{\mathbb{R}} g(k) \left|\Phi_k^{nr}(x)\right|^2 dk + \int_{\mathbb{R}} g(k) \left|\theta_k\right|^2 dk \left|u_I(x)\right|^2 . \tag{3.17}$$

The non resonant part of the wave function being regular with respect to k, the first integral above can be computed using a trapezoidal rule with coarse frequency mesh, reducing this way the number of Schrödinger equations to be solved. As remarked before, the resonance z_I has a small imaginary part. Therefore, it appears from formula (3.15), that the coefficient θ_k has a sharp peak when the wave function energy E_k is close to the resonant energy $\mathrm{Re}(z_I)$. The key-point in the present algorithm is then the approximation of the integral $\int_{\mathbb{R}} g(k) \left|\theta_k\right|^2 dk$.
For the sake of simplicity, the non resonant part of the wave function will be called non resonant wave function as well. The same remark holds for the time-dependent One Mode Approximation presented in section 4.2 below.

3.3.1 First method: One Mode Approximation

Consider a refined discretization $k_0 = -\kappa, k_1, ..., k_p, ..., k_P = \kappa$ of the interval $[-\kappa, \kappa]$ with uniform grid spacing Δk and suppose that there exist two integers P' and ν such that $\frac{P}{P'} = \nu$. Consider the large scale mesh $\hat{k}_{p'} = k_{\nu p'}$ for $p' = 0, ..., P'$ with uniform grid spacing $\Delta\hat{k} = \nu\Delta k$. Then, if we note $\Phi_{p',j}^{nr}$ the approximation of the non resonant wave function $\Phi_{k_{\nu p'}}^{nr}(x_j)$, $u_{I,j}$ the approximation of the resonant mode $u_I(x_j)$ and θ_p the approximation of the coefficient θ_{k_p}, the formula for the density is

$$n_{I,j} = \sum_{p'=0}^{P'-1} \left(g(\hat{k}_{p'}) \left|\Phi_{p',j}^{nr}\right|^2 + g(\hat{k}_{p'+1}) \left|\Phi_{p'+1,j}^{nr}\right|^2 \right) \frac{\Delta\hat{k}}{2} + \sum_{p=0}^{P-1} \left(g(k_p) \left|\theta_p\right|^2 + g(k_{p+1}) \left|\theta_{p+1}\right|^2 \right) \frac{\Delta k}{2} \left|u_{I,j}\right|^2$$

The crucial point which makes the algorithm faster is the reduction of the number of Schrödinger equations to be solved: P' equations instead of P equations for the Direct Resolution. However, this reduction implies that we only have access to the functions $\Phi_{p',j}^{nr}$ for $p' = 0, ..., P'$ and the computation of the coefficient θ_p, for $p \neq \nu p'$, requires an interpolation of the non resonant wave function in the right hand side of equation (3.15). It is provided by the piecewise constant interpolation formula below: for $p = 0, ..., P$

$$\theta_p = \frac{1}{z_I - E_p} v_0 \sum_{j \in w} \Phi_{p',j}^{nr} \overline{u_{I,j}} \Delta x \tag{3.18}$$

where $w = \{j \,|\, a_3 \leq x_j < b_3\}$, $E_p = E_{k_p}$ and $0 \leq p' \leq P'$ is the integer such that $p = \nu p' + r$ for some $0 \leq r \leq \nu - 1$. Since the evaluation of the coefficient θ_p in formula (3.18) is fast numerically, the number P can be chosen big enough to catch the resonance peak without a significant increase of the computational cost.

3.3.2 Second method: One Mode Approximation Integ

Is considered only the large scale frequency mesh introduced above: $\hat{k}_0, ..., \hat{k}_{P'}$. As noticed before, the integral of the non resonant part can be computed with a simple trapezoidal rule as follows

$$n_{I,j} = \sum_{p=0}^{P'-1} \left(g(\hat{k}_p) \left|\Phi_{p,j}^{nr}\right|^2 + g(\hat{k}_{p+1}) \left|\Phi_{p+1,j}^{nr}\right|^2 \right) \frac{\Delta\hat{k}}{2} + \sum_{p=0}^{P'-1} J_p \left|u_{I,j}\right|^2 \tag{3.19}$$

where $J_p := \int_{\hat{k}_p}^{\hat{k}_{p+1}} g(k)\,|\theta_k|^2\,dk$. The required precision for the density is reached thanks to an adapted treatment of the integral in J_p. It follows from (3.15) that:

$$J_p = \int_{\hat{k}_p}^{\hat{k}_{p+1}} S_k \frac{k}{|E_k - z_I|^2} dk\,,$$

where

$$S_k = \frac{g(k)}{k} v_0^2 \left| \int_{a_3}^{b_3} \Phi_k^{nr} \overline{u_I} dx \right|^2 .$$

We observe numerically that $\|\Phi_k^{nr}\|_{L^\infty(0,L)} = \mathcal{O}(k)$ when k tends to 0 which is shown theoretically in [19] in the particular case k tends to 0^+ using an additional condition on the potential. Therefore, we consider that S_k is a smooth function of the variable k in a small neighborhood of 0. Since the wave function Φ_k^{nr} has no resonance peak, the function S_k is also a smooth function of k outside such a neighborhood. As a consequence, S_k can be approximated by a constant on $[\hat{k}_p, \hat{k}_{p+1}]$ which gives:

$$J_p = S_p \int_{\hat{k}_p}^{\hat{k}_{p+1}} \frac{k}{|E_k - z_I|^2} dk\,,$$

where

$$S_p := \frac{g\left(\hat{k}_p\right)}{\hat{k}_p} v_0^2 \left| \sum_{j \in w} \Phi_{p,j}^{nr} \overline{u_{I,j}} \Delta x \right|^2 ,$$

and w is defined in section 3.3.1. The resonance z_I can be written

$$z_I = E_I - i\Gamma_I \tag{3.20}$$

where $E_I \in I\!R$ and $\Gamma_I > 0$. Under the assumption $0 \notin [\hat{k}_p, \hat{k}_{p+1}]$, it holds $E_k = \frac{\hbar^2 k^2}{2m} - B_p$ on $[\hat{k}_p, \hat{k}_{p+1}]$ where B_p is a constant equal to 0 or B_I. Then, it follows:

$$J_p = S_p \int_{\hat{k}_p}^{\hat{k}_{p+1}} \frac{k}{\left(\frac{\hbar^2 k^2}{2m} - B_p - E_I\right)^2 + \Gamma_I^2} dk\,.$$

Utilizing the change of variable $E = \frac{\hbar^2 k^2}{2m} - B_p - E_I$ in the integral above, the approximation of J_p follows:

$$J_p = \frac{m S_p}{\hbar^2 \Gamma_I} \left(\arctan\left(\frac{\hat{E}_{p+1} - E_I}{\Gamma_I} \right) - \arctan\left(\frac{\hat{E}_p - E_I}{\Gamma_I} \right) \right) \quad \text{for} \quad p = 0, ..., P' \tag{3.21}$$

where $\hat{E}_p := E_{\hat{k}_p}$. The above approximation of J_p will be used regardless of the verification of the assumption $0 \notin [\hat{k}_p, \hat{k}_{p+1}]$. It provides an accurate treatment of the resonance peak even if $\Delta\hat{k}$ is large. The approximation of the density follows by replacing (3.21) in (3.19).

Remark 3.2. The computational time of the One Mode Approximation algorithm can be reduced when the method to compute the resonance, in section 3.2, is the fundamental mode and fundamental energy (u_D, E_D), of the Dirichlet Hamiltonian (3.16), only for the first iteration $l = 0$ of the Gummel algorithm 3.1. Indeed, for $l \geq 1$, the computation of (u_D, E_D) is avoided by initializing the method at the resonant mode and resonance obtained at the previous iteration: $l - 1$.

Remark 3.3. The size of the grid spacing Δk for the refined frequency mesh is chosen numerically. It can be estimated analytically by imposing that, around the resonance energy E_I, the difference $E_{p+1} - E_p$ is smaller than half the peak width Γ_I.

4 The time-dependent algorithm

This section deals with the time evolution of the system under a time-dependent applied bias $B(t)$ as in Figure 1. We will consider only the case of the step like bias of the form:

$$B(t) = \begin{cases} B_I, & t = 0 \\ B_\infty, & t > 0 \end{cases} \tag{4.1}$$

where $B_I, B_\infty \geq 0$ and $B_I \neq B_\infty$. The case of the general bias requires an adaptation of the discrete transparent boundary conditions for the resolution of the transient Schrödinger equation. It will not be treated in this paper.

4.1 The algorithm

As in the stationary regime, we first present the algorithm proposed in [38] to solve the time-dependent nonlinear Schrödinger-Poisson system (2.1)(2.2)(2.3). Then, we give the details of a time-dependent One Mode Approximation algorithm.
The space and frequency meshes are defined as in section 3.1. In order to verify the condition (C.15) for all $k \in [-\kappa, \kappa]$, the time step Δt is chosen such that:

$$\Delta t < \frac{\pi\hbar}{2\left(\frac{\hbar^2\kappa^2}{2m} + \sup_{t\geq 0} B(t)\right)}\,. \tag{4.2}$$

Then, for a given exterior potential $U(t)$, the algorithm corresponds to the computation of the sequence V^l of approximations of the self-consistent potential at time $t_l = l\Delta t$. The initial potential V^0, resp. wave function Ψ_p^0, is given by V_I, and resp. Φ_{k_p}, solution to the stationary Schrödinger-Poisson system (2.5)(2.9)(2.10) with exterior potential equal to U_I. The Schrödinger equation (2.1) is solved using a Crank-Nicolson type scheme and, in our nonlinear framework, a choice of the intermediary potential $V^{l+\frac{1}{2}}$ which preserves the unconditional stability of the semi-implicit scheme is required. As it will be shown in section 5.3.1, the extrapolation:

$$V^{l+\frac{1}{2}} = 2V^l - V^{l-\frac{1}{2}} \tag{4.3}$$

proposed in [38] gives accurate results for small time steps, however, the same accuracy is possible for bigger time steps by setting:

$$V^{l+\frac{1}{2}} = \frac{3}{2}V^l - \frac{1}{2}V^{l-1}\,. \tag{4.4}$$

The extrapolation (4.4) is proposed in [17] and corresponds to a modified Adams-Bashforth-Crank-Nicolson method. Then, the algorithm writes:

Algorithm 4.1 (Transient algorithm)**.**

Do For $l = 0$ to $l_{tot} - 1$:

Computation of the intermediary potential
Computation of the potential $V^{l+\frac{1}{2}}$ from the potentials V^l and V^{l-1} using (4.4) with the convention $V^{-1} = V^0$.

Computation of the density

*S*1. For $p = 0, ..., P$: computation of the wave function Ψ_p^{l+1}, solution to (2.1) at time t^{l+1} and frequency k_p, using the potential $V^{l+\frac{1}{2}}$ and the wave function Ψ_p^l.

*S*2. Numerical integration: for $j = 0, ..., J$

$$n_j^{l+1} = \sum_{p=0}^{P-1} \left(g(k_p) \left|\Psi_{p,j}^{l+1}\right|^2 + g(k_{p+1}) \left|\Psi_{p+1,j}^{l+1}\right|^2 \right) \frac{\Delta k}{2} \tag{4.5}$$

Coupling, Poisson equation
Computation of the potential V^{l+1} from the density n^{l+1} by solving the Poisson equation (2.2):

$$\begin{cases} -\partial_x^2 V^{l+1} = \frac{q^2}{\varepsilon}(n^{l+1} - n_D), \quad (0, L) \\ V^{l+1}(0) = V^{l+1}(L) = 0\,. \end{cases} \tag{4.6}$$

End Do.

In equation (4.5), n_j^{l+1} denotes the approximation of the density $n^{l+1}(x_j)$ and $\Psi_{p,j}^{l+1}$ the approximation of the wave function $\Psi_p^{l+1}(x_j)$. The linear equation (4.6) is discretized with finite difference and solved by a simple matrix inversion. Due to the presence of resonances, the steps $S1$ and $S2$ to compute the density will be crucial here also.
In the algorithm proposed in [38], which we will call equally Direct Resolution, the step $S1$ is performed as follows: the function Ψ_p^{l+1} is computed on $[0, L]$ using Ψ_p^l and $V^{l+\frac{1}{2}}$ by the resolution of (2.1) with the Crank-Nicolson scheme (C.2), where the potential Q is equal to $U + V$. Since the initial data Φ_{k_p} is not supported only in $[0, L]$, suitable boundary conditions are the non-homogeneous discrete transparent boundary conditions (C.9)(C.12). Because no particular treatment of the resonances is applied in step $S1$, the accuracy of the method is provided in step $S2$ by the imposition of a small uniform grid spacing Δk in the trapezoidal rule (4.5). Indeed, if the grid spacing is small only near the initial resonant frequencies, the refined mesh will loose its relevance because of the time evolution of the resonance. Therefore, the stationary Adaptive Method does not extend to the transient regime and, if no additional treatment is performed (a strategy would be to choose a small frequency grid spacing only in the regions where will live the resonance peaks), the number of Schrödinger equations to be solved have to be important in the time-dependent Direct Resolution. Moreover, in addition to a matrix inversion, which is equally required in the stationary case, each time-dependent Schrödinger equation requires discrete convolutions of sequences whose size, smaller than the time iteration number l, has to be balanced to preserve the accuracy of the method, see equations (C.9)(C.12) and (C.21)(C.22). This increases the numerical cost of one time step and can make the time-dependent simulations very long: actually, due to the condition (4.2), the time step must be chosen much smaller than the scaling time of the system and the number l can become very big. In this context, it is important to look for an adapted treatment of the resonance peaks to reduce the number of frequency points.
In the following section, we propose a One Mode Approximation method which extends the method proposed in section 3.3 to the time-dependent case.

4.2 The time-dependent One Mode Approximation

Recall first that in the initial work [40], the One Mode Approximation was presented in the time-dependent case with a simplified model. Then, let us start with the description, in the One Mode Approximation, of the decomposition of a wave function $\Psi_k(t)$ solution to the transient Schrödinger equation (2.1) for a given frequency k. The One Mode Approximation consists in the decomposition:

$$\Psi_k(t) = \Psi_k^{nr}(t) + \Psi_k^r(t)\,, \tag{4.7}$$

where the non resonant part $\Psi_k^{nr}(t)$ solves the transient Schrödinger equation:

$$\begin{cases} i\hbar\partial_t \Psi_k^{nr}(t) = [-\frac{\hbar^2}{2m}\partial_x^2 + U_{fill}(t) + V(t)]\Psi_k^{nr}(t), \quad x \in I\!R \\ \Psi_k^{nr}(0) = \Phi_k^{nr}\,, \end{cases} \tag{4.8}$$

with filled potential $U_{fill}(t) = U(t) + v_0 \mathbf{1}_{[a_3,b_3]}$ and Φ_k^{nr} is solution to (3.12) with the initial potential $U_{I,fill} + V_I$. Using the same argument as in the stationary regime, we look for $\Psi_k^r(t)$ proportional to the resonant mode $u(t)$ corresponding to the first resonance $z(t)$ of the Hamiltonian $H(t)$ at time t: in other words

$$\Psi_k^r(t, x) = \lambda_k(t) u(t, x), \quad x \in [0, L] \tag{4.9}$$

where

$$[-\frac{\hbar^2}{2m}\partial_x^2 + U(t) + V(t)]u(t) = z(t)u(t) \tag{4.10}$$

and $\int_0^L |u(t,x)|^2 dx = 1$. If u_I and θ_k are respectively the resonant mode and the proportionality coefficient given by (3.13) and (3.15), then it holds from (3.11)(3.14):

$$\Phi_k(x) = \Phi_k^{nr}(x) + \theta_k u_I(x), \quad x \in [0, L]\,. \tag{4.11}$$

Comparing (4.7)(4.9) and (4.11), the initial condition in (2.1) and (4.8) imply $\lambda_k(0) = \theta_k$. Moreover, injecting (4.7)(4.9) in the transient Schrödinger equation (2.1), and utilizing the equations (4.8) and (4.10), we get the following equation on $\lambda_k(t)$:

$$[i\hbar\lambda_k'(t) - z(t)\lambda_k(t)]u(t,x) + i\hbar\lambda_k(t)\partial_t u(t,x) = -v_0 \mathbf{1}_{[a_3,b_3]}(x)\Psi_k^{nr}(t,x).$$

Multiplying the previous equation by $\overline{u}(t,x)$ and integrating on $(0,L)$, it follows:

$$\begin{cases} \lambda_k'(t) + [\frac{i}{\hbar}z(t) + \int_0^L \partial_t u(t,x)\overline{u}(t,x)dx]\lambda_k(t) = \frac{i}{\hbar}v_0 \int_{a_3}^{b_3} \Psi_k^{nr}(t,x)\overline{u}(t,x)dx \\ \lambda_k(0) = \theta_k \end{cases} \tag{4.12}$$

Remark 4.2. In the linear case, obtained by taking $V(t) = 0$ in (2.1), it holds for $t > 0$: $u(t) = u_\infty$ and $z(t) = E_\infty - i\Gamma_\infty$, where $E_\infty \in I\!R$ and $\Gamma_\infty > 0$. Then, under the assumption $\Psi_k^{nr}(t,x) = \tilde{\Psi}_k^{nr}(x)e^{-i\frac{\varepsilon_k^\infty}{\hbar}t}$ where

$$\varepsilon_k^\infty = \begin{cases} \frac{\hbar^2 k^2}{2m}, & k \geq 0 \\ \frac{\hbar^2 k^2}{2m} - B_\infty, & k < 0 \end{cases}, \tag{4.13}$$

equation (4.12) is an ODE which homogeneous solution is oscillating with angular frequency $\frac{E_\infty}{\hbar}$ and source term with angular frequency $\frac{\varepsilon_k^\infty}{\hbar}$. Therefore $\lambda_k(t)$ has a peak at the frequencies k such that $\varepsilon_k^\infty = E_\infty$. Due to the initial condition in (4.12), one expects a coexistence of this peak with a second peak at the frequencies k such that $E_k = E_I$ with decay rate $\frac{\Gamma_\infty}{\hbar}$, where E_k and E_I are given by (2.8) and (3.20). This is verified numerically in section 5.3.4.

4.2.1 Step $S1$

The aim here is to compute the elements of the decomposition (4.7)(4.9) at the time $t = t^{l+1}$. At this point of the algorithm, we do not have the value of the potential V^{l+1} and the corresponding resonant mode u^{l+1} can not be computed. Therefore, we will make the following approximation for the wave function at time t^{l+1} and frequency k:

$$\Psi_k^{l+1} = \Psi_k^{nr,l+1} + \lambda_k^{l+1} u^{l+\frac{1}{2}}\,. \tag{4.14}$$

Then the step $S1$ writes as follows: Suppose that the quantities $\Psi_k^{nr,l}$ and λ_k^l are known (at $l = 0$, it is given by the initial decomposition (4.11)).
As it is done in the Direct Resolution for Ψ_k^{l+1}, the non resonant wave function $\Psi_k^{nr,l+1}$ at time t^{l+1} and frequency k is computed on $[0, L]$ using $\Psi_k^{nr,l}$ and $V^{l+\frac{1}{2}}$ by the resolution of (4.8) with the Crank-Nicolson scheme (C.2) where the potential Q is equal to $U_{fill} + V$ and the initial data Φ is equal to Φ_k^{nr}. Equation (C.2) comes, in particular, with the transparent boundary conditions (C.9)(C.12).
The resonant mode $u^{l+\frac{1}{2}}$ and the resonance $z^{l+\frac{1}{2}}$ are computed using the method presented in section 3.2 where the potential Q is equal to $U^{l+\frac{1}{2}} + V^{l+\frac{1}{2}}$ and $U^{l+\frac{1}{2}} = U(t^{l+\frac{1}{2}})$. The initial guess for $(u^{l+\frac{1}{2}}, z^{l+\frac{1}{2}})$ are the first eigenfunction and eigenenergy of the Hamiltonian

$$[-\frac{\hbar^2}{2m}\partial_x^2 + U^{l+\frac{1}{2}} + V^{l+\frac{1}{2}}] \tag{4.15}$$

with homogeneous Dirichlet boundary conditions at a_2 and b_2.
To achieve the step $S1$, we have to compute the coefficient λ_k^{l+1} at time t^{l+1} and frequency k. It is obtained from λ_k^l, $\Psi_k^{nr,l}$, $\Psi_k^{nr,l+1}$, $z^{l+\frac{1}{2}}$ and $u^{l+\frac{1}{2}}$ by the resolution of equation (4.12). This resolution is performed with a trapezoidal rule, which leads to the following iteration:

$$(\lambda_k^{l+1}-\lambda_k^l)/\Delta t+[\frac{i}{\hbar}z^{l+\frac{1}{2}}+\int_0^L \partial_t u^{l+\frac{1}{2}}\overline{u^{l+\frac{1}{2}}}dx](\lambda_k^l+\lambda_k^{l+1})/2 \\ = \frac{iv_0}{2\hbar}\int_{a_3}^{b_3}\left[\Psi_k^{nr,l}+\Psi_k^{nr,l+1}\right]\overline{u^{l+\frac{1}{2}}}dx \quad (4.16)$$

where $\partial_t u^{l+\frac{1}{2}}$ stands for $\partial_t u(t^{l+\frac{1}{2}})$. By adequately fixing the resonant mode phase, the quantity

$$\mu^{l+1/2}:=\int_0^L \partial_t u^{l+1/2}\overline{u^{l+1/2}}dx \quad (4.17)$$

appearing in (4.16) is fitted to zero. Given $\tilde{u}^{l+1/2}$ resonant mode of lower energy of the Hamiltonian (4.15), verifying $\|\tilde{u}^{l+1/2}\|_{L^2(0,L)}=1$, we look for $u^{l+1/2}$ of the form $u^{l+1/2}=\tilde{u}^{l+1/2}e^{i\varphi^{l+1/2}}$ where $\varphi^{l+1/2}\in I\!R$ is such that the wanted property holds. We note first that we have the approximation

$$\mu^{l+1/2}=\frac{1}{2\Delta t}\int_0^L (u^{l+1/2}-u^{l-1/2})\overline{(u^{l+1/2}+u^{l-1/2})}dx\,,$$

which becomes

$$\mu^{l+1/2}=\frac{i}{\Delta t}\mathrm{Im}[\int_0^L u^{l+1/2}\overline{u^{l-1/2}}dx] \quad (4.18)$$

under the condition $\|u^{l-1/2}\|_{L^2(0,L)}=\|u^{l+1/2}\|_{L^2(0,L)}=1$. Then, defining

$$\omega^{l+1/2}=\int_0^L \tilde{u}^{l+1/2}\overline{u^{l-1/2}}dx\,, \quad (4.19)$$

we choose

$$e^{i\varphi^{l+1/2}}=\frac{\overline{\omega^{l+1/2}}}{|\omega^{l+1/2}|}$$

and it follows:

$$\int_0^L u^{l+1/2}\overline{u^{l-1/2}}dx=e^{i\varphi^{l+1/2}}\int_0^L \tilde{u}^{l+1/2}\overline{u^{l-1/2}}dx=\omega^{l+1/2}e^{i\varphi^{l+1/2}}=|\omega^{l+1/2}|\in I\!R\,.$$

As a consequence, $\mathrm{Im}[\int_0^L u^{l+1/2}\overline{u^{l-1/2}}dx]=0$ and equation (4.18) shows that $u^{l+1/2}$ is such that $\mu^{l+1/2}$ is almost equal to 0. In applications, the space integral in (4.19) is computed using a rectangle method.

Remark 4.3. As it is proposed in the stationary case, see Remark 3.2, the algorithm can be accelerated by choosing, for $l\geq 1$, $(u^{l-\frac{1}{2}},z^{l-\frac{1}{2}})$ as initial guess of the method to compute $(u^{l+\frac{1}{2}},z^{l+\frac{1}{2}})$. When $l=0$, the initial guess is the resonant mode and the resonance given by the stationary solution.

Remark 4.4. Although it is harder to implement than an explicit Euler method, the semi-implicit trapezoidal rule (4.16), used to solve the stiff-like equation (4.12), is required for stability purposes. Indeed, the imaginary part of the resonance $z(t)$ being strictly negative, the ODE (4.12) is similar to the test equation: $y'=\alpha y$ where $\mathrm{Re}\,(\alpha)<0$, for which the trapezoidal rule solution is bounded independently of the time step whereas the Euler explicit solution is conditionally bounded. In particular, as explained above, the quantity $\mu^{l+1/2}$ defined in (4.17) can been fitted to zero in (4.16), and a straightforward calculation shows that the resulting algorithm is unconditionally stable, in the sens that for all $N\geq 0$

$$\left|\lambda_k^l\right|\leq\left|\lambda_k^0\right|+T\max_{0\leq n\leq N-1}\left|\frac{iv_0}{2\hbar}\int_{a_3}^{b_3}\left[\Psi_k^{nr,n}+\Psi_k^{nr,n+1}\right]\overline{u^{n+\frac{1}{2}}}dx\right|,\quad 0\leq l\leq N$$

where $T=N\Delta t$.

4.2.2 Step $S2$

The step $S2$ is performed using the decomposition (4.14) to find an approximation of the density n_j^{l+1} in (4.5) which is adapted to the resonant peaks. Like in section 3.3, we make the approximation:

$$\left|\Psi_k^{l+1}(x)\right|^2 = \left|\Psi_k^{nr,l+1}(x)\right|^2 + \left|\lambda_k^{l+1}\right|^2 \left|u^{l+\frac{1}{2}}(x)\right|^2 . \tag{4.20}$$

The non resonant wave function Ψ_k^{nr} is regular with respect to the frequency k and the integral of the first term in (4.20) can be computed using a trapezoidal rule with coarse frequency mesh. As noticed in Remark 4.2, the coefficient λ_k has sharp peaks at resonant frequencies and the frequency mesh is taken thin for the integral of the second term in (4.20). More precisely, we consider the frequency meshes $\{\hat{k}_{p'},\, p' = 0, ..., P'\}$ and $\{k_p,\, p = 0, ..., P\}$ introduced in section 3.3.1 and which have different scales adjusted using the ratio $\nu = \frac{P}{P'} \in \mathbb{N}$. Then, if we note $\Psi_{p',j}^{nr,l}$ the approximation of the non resonant wave function $\Psi_{k_{\nu p'}}^{nr,l}(x_j)$, λ_p^l the approximation of the coefficient $\lambda_{k_p}^l$ and $u_j^{l+\frac{1}{2}}$ the approximation of the resonant mode $u^{l+\frac{1}{2}}(x_j)$, the formula for the density is

$$n_j^{l+1} = \sum_{p'=0}^{P'-1} \left(g(\hat{k}_{p'}) \left|\Psi_{p',j}^{nr,l+1}\right|^2 + g(\hat{k}_{p'+1}) \left|\Psi_{p'+1,j}^{nr,l+1}\right|^2 \right) \frac{\Delta \hat{k}}{2}$$
$$+ \sum_{p=0}^{P-1} \left(g(k_p) \left|\lambda_p^{l+1}\right|^2 + g(k_{p+1}) \left|\lambda_{p+1}^{l+1}\right|^2 \right) \frac{\Delta k}{2} \left|u_j^{l+\frac{1}{2}}\right|^2 . \tag{4.21}$$

The number of Schrödinger equations to solve is reduced, P' equations instead of P equations for the Direct Resolution, and the numerical cost is reduced. However, this reduction implies that we have only access to the functions $\Psi_{p',j}^{nr,l}$ for $p' = 0, ..., P'$ and the computation of the coefficient λ_p^{l+1}, for $p \neq \nu p'$, requires an interpolation of the non resonant wave function to evaluate the source term in (4.16). If we set $\varepsilon_p^\infty = \varepsilon_{k_p}^\infty$ where ε_k^∞ is given by (4.13), it follows from Remark 4.2 that the coefficient λ_p^{l+1} has a peak when the energy ε_p^∞ is equal to E^{l+1} (lower resonant energy corresponding to the potential V^{l+1}) only if the approximation of the source term in (4.16) includes the time oscillations of the non resonant wave function. In particular, a polynomial interpolation of the non resonant wave function is not adapted. Solving equation (4.16) and performing an oscillatory interpolation of the non resonant wave function, we obtain the following suitable algorithm which extends the formula (3.18) to the time-dependent case: for $p = 0, ..., P$

$$\lambda_p^{l+1} = \frac{1}{1 + i\frac{\Delta t z^{l+\frac{1}{2}}}{2\hbar}} \left[\left(1 - i\frac{\Delta t z^{l+\frac{1}{2}}}{2\hbar} \right) \lambda_p^l \right.$$
$$\left. + \frac{i v_0 \Delta t}{2\hbar} \sum_{j \in w} \left(\tilde{\Psi}_{p',j}^{nr,l} e^{-i\omega_p^\infty t^l} + \tilde{\Psi}_{p',j}^{nr,l+1} e^{-i\omega_p^\infty t^{l+1}} \right) \overline{u_j^{l+\frac{1}{2}}} \Delta x \right] \tag{4.22}$$

where w is defined in section 3.3.1 and $0 \leq p' \leq P'$ is the integer such that $p = \nu p' + r$ for some $0 \leq r \leq \nu - 1$. The amplitude-like function appearing in equation (4.22) is defined by

$$\tilde{\Psi}_{p',j}^{nr,l} = \Psi_{p',j}^{nr,l} e^{i\omega_{\nu p'}^\infty t^l}$$

and

$$\omega_p^\infty = \frac{\varepsilon_p^\infty}{\hbar} . \tag{4.23}$$

Remark 4.5. The condition (4.2) insures that the time step is small enough with respect to one period of the oscillating term $e^{-i\omega_p^\infty t}$ in (4.22). The time-dependent One Mode Approximation extends the method in section 3.3.1 and it is numerically verified that it is stable in time and allows long time simulations, see section 5.3.3. On the other hand, due to the function $e^{-i\omega_p^\infty t}$, a time-dependent extension of the method presented in 3.3.2 is not obvious and gives a non-stable algorithm if no particular treatment is performed.

Remark 4.6. In section C.2, we remarked that the accuracy of the algorithm is improved by replacing the angular frequencies (C.8)(C.11) by the discrete ones (C.13)(C.14) in the boundary conditions (C.9)(C.12). Similarly, the accuracy of the time-dependent One Mode Approximation is improved when the angular frequency (4.23) is replaced by the discrete one below:

$$\omega_p^\infty = \frac{2}{\Delta t} \arctan\left(\frac{\Delta t \varepsilon_p^\infty}{2\hbar}\right). \tag{4.24}$$

5 Results

The physical parameters used for the numerical computations are gathered in the following array:

Rel. el. mass	0.067	Rel. permitivity	11.44
Temperature	$300\,K$	Fermi level E_F	$6,7097 \times 10^{-21}\,J$
Donor density n_D^1	$10^{24}\,m^{-3}$		
Donor density n_D^2	$5 \times 10^{21}\,m^{-3}$		

For all the tests, the two barriers has the same size which is equal to the size of the well. The external potential is determined by Figure 1 and the data below:

$L\,(nm)$	$a_1\,(nm)$	$a_2\,(nm)$	$a_3\,(nm)$	$b_3\,(nm)$	$b_2\,(nm)$	$b_1\,(nm)$	$v_0\,(eV)$
135	50	60	65	70	75	85	0.3

In all the simulations, we fixed $\kappa = \sqrt{\frac{2m}{\hbar^2}(E_F + 7k_BT)}$ and we took the number of space points to be $J = 300$ which is such that the condition (3.2) is verified. In what follows, the CPU time is the amount of time for which the central processing unit was used for processing the algorithm presented.

5.1 Computation of resonances

In this section, we give the numerical values of the resonance of lower energy obtained using the algorithm presented in section 3.2 for different biases B_I. The potential Q is equal to $U_I + V_I$ where U_I is the external potential corresponding to B_I and V_I the corresponding solution to the Schrödinger-Poisson system (2.5)(2.9)(2.10) given by the Direct Resolution, with $P = 3750$, as described in section 5.2. We obtain the following results:

$B_I\,(eV)$	N_{cv}	$E_D\,(meV)$	$E_I\,(meV)$	Γ_I/E_I
0	3	135.14	134.71	1.7030×10^{-3}
0.1	3	88.524	88.090	2.7547×10^{-3}

where the number of iterations before convergence N_{cv} denotes the iteration n of the algorithm such that $|M(z^n)u^n|_2 < 10^{-15}$, E_D denotes the fundamental energy of the Dirichlet Hamiltonian (3.16) and the resonance is equal to $z_I = E_I - i\Gamma_I$. The modulus of the normalized resonant mode for $B_I = 0.1\,eV$ is represented in Figure 2.

This section provides a numerical verification of the following theoretical results, which were used to write the One Mode Approximation: E_D is close to E_I, Γ_I is small with respect to E_I and the restriction of the resonant mode to the interval $[0, L]$ is small outside the island $[a_2, b_2]$.

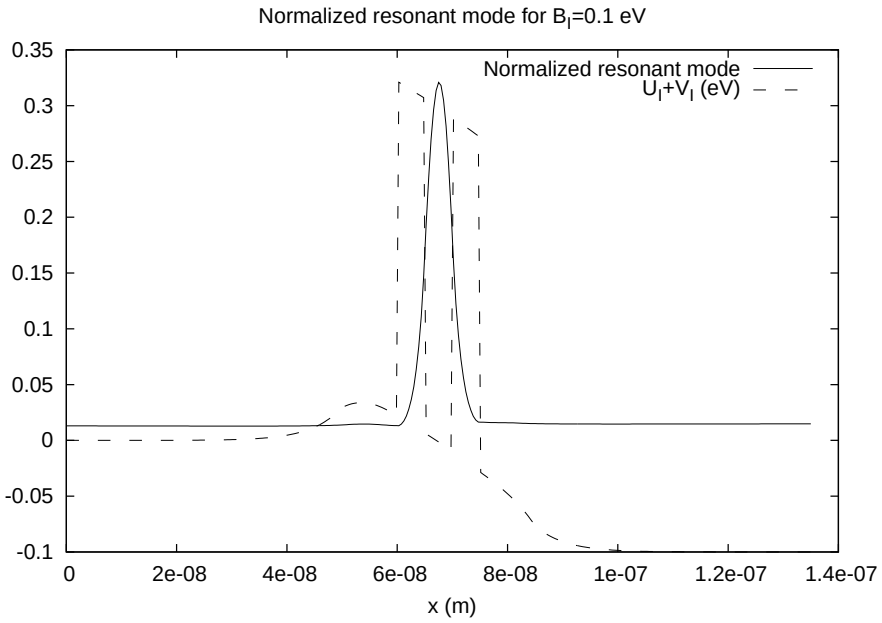

Figure 2: Representation of the potential $U_I + V_I$ (dashed line) and the corresponding normalized resonant mode $\frac{|u_I(x)|}{|u_I|_2}$ (full line) for $B_I = 0.1\ eV$.

5.2 The stationary regime

We give here a numerical comparison of the methods presented in section 3: the Direct Resolution, Adaptive Method, One Mode Approximation and One Mode Approximation Integ. The Direct Resolution plays the role of the reference method. For all the tests, the reference potential in (3.1) is given in electron-volts by $V_{ref} = \frac{Tk_B}{q}$.

Remark 5.1. For the bias $B_I = 0$, the Gummel algorithm 3.1 can be initialized at the potential $V_I^0 = 0$. For $B_I > 0$, such an initialization does not converge and we have convergence when the initial potential is the solution given by the method for $B_I = 0$.

As it was underlined in section 3.1, the choice of the frequency mesh determines the convergence and the numerical cost of the method. In particular, for the Direct Resolution, it is verified numerically that, $P \geq 3700$ is required to insure the convergence of the method for the biases $B_I = 0\,eV$ and $B_I = 0.1\,eV$. This fact is illustrated in Figure 3 for $B_I = 0\,eV$.

Indeed, for $P = 1500$, after 40 iterations the method fails to converge for a CPU time equal to $1.8241\,s$. For $P = 3750$, the method converges: the difference Δ becomes less than $tol = 10^{-14}$ after 34 iterations for a CPU time equal to $3.8562\,s$. For the Direct Resolution, it appears that a big number of frequency points, and therefore a relatively hight numerical cost, is required to have convergence. This remark enhances the importance of the alternative methods.

The results given by the different methods, for two different values of the bias B_I, are given in Figure 4 and Table 1. For the Adaptive Method, the small step size is equal to $\Delta k = \frac{2\kappa}{4500}$ and the large step size is equal to $12\Delta k$. The step size is equal to the small one when the logarithmic derivative of the transmission coefficient, see [38, 19] for its explicit formula, is greater than $1.3L$. The number of frequency points changes from an iteration to the other, however it stays around a fixed number which is 587 for $B_I = 0\,eV$ and 535 for $B_I = 0.1\,eV$. For the other methods, the frequency mesh is given by the integers $P = 3750$ and $P' = 150$.

In Table 1, the integer N_{cv} is the total number of iterations of Algorithm 3.1 for the tolerance tol $= 10^{-14}$. The column CPU denotes the CPU time of the method and the column *Dist to*

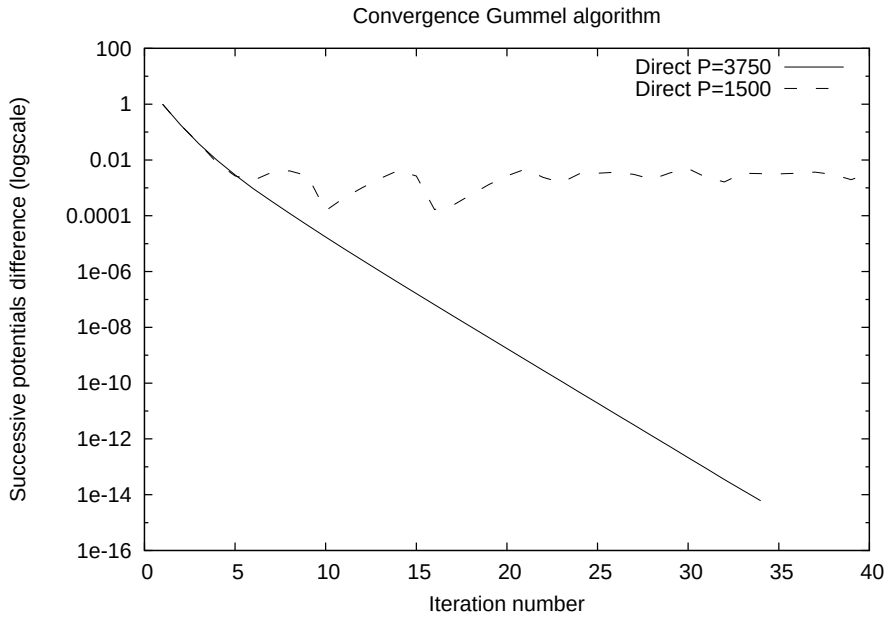

Figure 3: Successive potentials difference Δ defined by (3.4) with respect to the number of iterations of Algorithm 3.1 for the Direct Resolution, for $B_I = 0\,eV$, and for the values $P = 1500$ and $P = 3750$.

		N_{cv}	CPU(s)	Dist to reference (%)
$B_I = 0\,eV$	Direct	34	3.8642	/
	Adaptive	34	0.6040	1.3859×10^{-2}
	One Mode	34	0.6440	0.2561
	One Mode Integ	34	0.6040	0.3700
$B_I = 0.1\,eV$	Direct	31	3.3402	/
	Adaptive	31	0.4800	4.9157×10^{-3}
	One Mode	31	0.5560	0.7689
	One Mode Integ	31	0.4880	0.5126

Table 1: Comparison of the Direct Resolution, Adaptive Method, One Mode Approximation and One Mode Approximation Integ methods for the resolution of the stationary Schrödinger-Poisson system (2.5)(2.9)(2.10) for $B_I = 0\,eV$ and $B_I = 0.1\,eV$.

$B_I = 0\,eV$

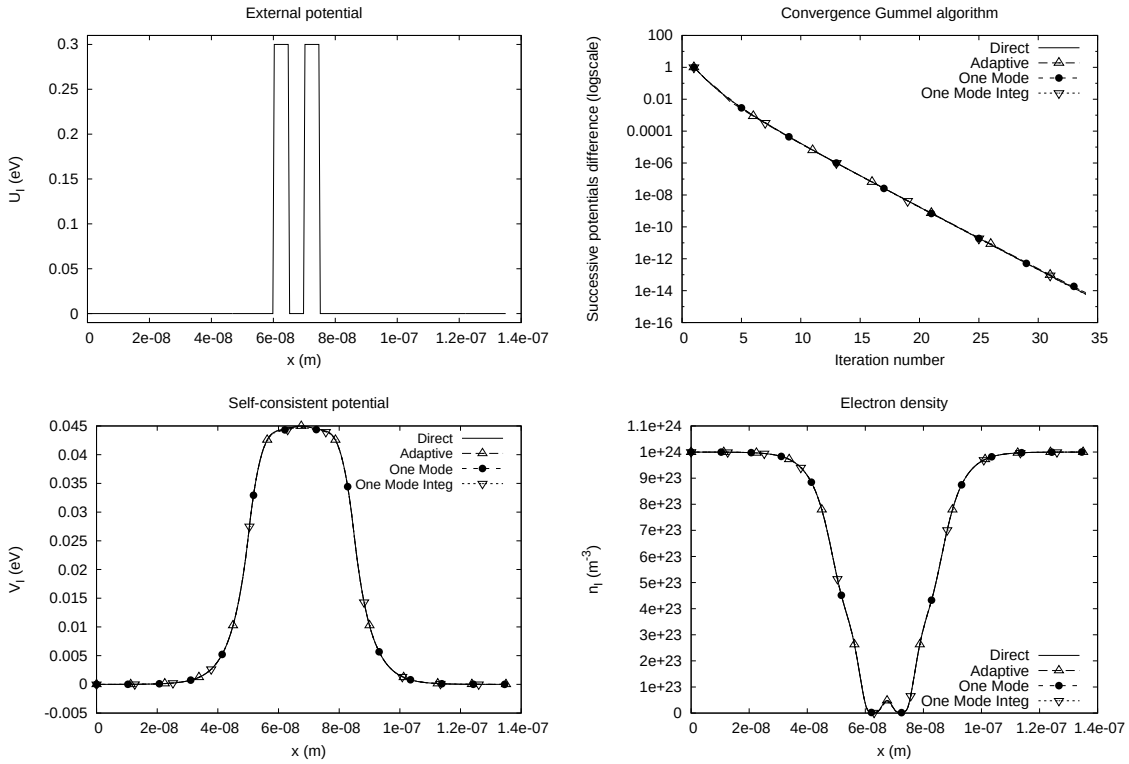

$B_I = 0.1\,eV$

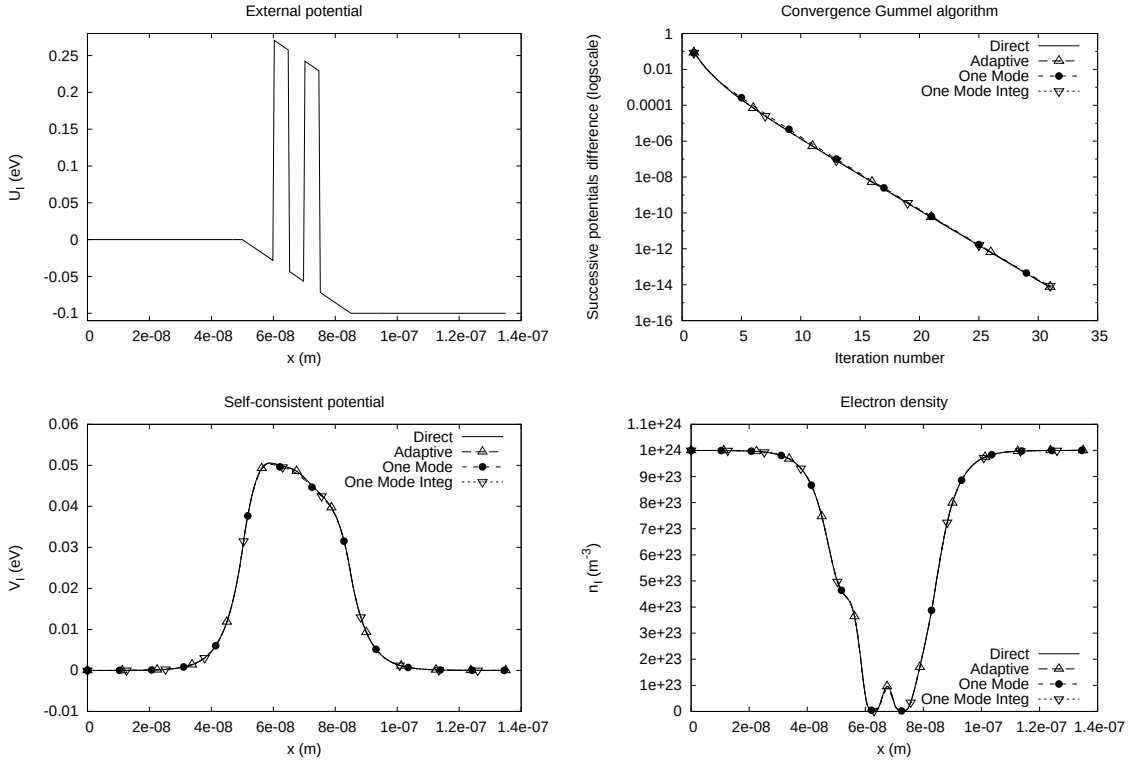

Figure 4: For the biases $B_I = 0\,eV$ and $B_I = 0.1\,eV$ and, for the methods considered, are represented from left to right: The external potential U_I, The corresponding successive potentials difference Δ defined by (3.4) with respect to the number of iterations of Algorithm 3.1, The self-consistent potential V_I after convergence, and The electron density n_I after convergence.

reference, the l^2-norm relative distance to the reference method potential. The last is given by:

$$100\frac{\left|V^{N_{cv}} - V_{di}\right|_2}{|V_{di}|_2},$$

where V_{di} is the potential of the Direct Resolution.
It appears from Figure 4 and Table 1 that the alternative methods converge as fast as the reference method in term of number of iterations, and give a solution very close to the reference solution, for a smaller CPU time. For the alternative methods, by adequately fixing the parameters, and possibly allowing a bigger value in the column *Dist to reference* in Table 1, the frequency mesh can be chosen such that the CPU time is reduced. Anyway, for the frequency meshes chosen here, the alternative methods are an improvement to the reference method since their CPU times are lower than the CPU time of the Direct Resolution for the lowest value of P such that the convergence of the method is ensured for the biases considered.
Although the One Mode Approximation and One Mode Approximation Integ methods require less frequency points than the Adaptive Method, the computation of the second term on the right-hand side of equation (3.17) increases the numerical cost of the two first methods, such that the three alternative methods have an equivalent CPU time. On the other hand, compared to the other alternative methods, the Adaptive Method provides a self-consistent potential which is closer to the Direct Resolution potential (this is probably due to the fact that the step $S1$ is performed in the same way for the two last methods). However, in the present work, the One Mode Approximation is more interesting than the other alternative methods since, as remarked earlier, the last can not be generalized to the time-dependent case and since the time-dependent Direct Resolution is time-consuming for the reasons given in section 4.1.

5.3 The transient regime

For all the tests, the external potential $U(t)$ is the time-dependent external potential corresponding to the bias $B(t)$ defined in (4.1) where $B_I = 0\,eV$, $B_\infty = 0.1\,eV$.

5.3.1 Direct resolution: Toward optimal parameters

The Direct Resolution presented in section 4.1 will play the role of the reference method and its CPU time is essential to measure the effective improvement provided by our alternative method. In this context, we show in the present section which choice of the parameters of the Direct Resolution allows a reduction of the CPU time of the method while conserving a reasonable accuracy.
The initial data of the method is given by the stationary Direct Resolution for the initial bias $B_I = 0\,eV$ and the parameters given in section 5.2 where $P = 3750$. The stationary potential corresponding to the final bias B_∞ is computed in the same way and will be denoted V_∞.
For different parameters of the method, is represented in Figure 5 the time evolution of the l^2-norm relative distance to the potential V_∞:

$$100\frac{\left|V^l - V_\infty\right|_2}{|V_\infty|_2}, \tag{5.1}$$

where V^l is the Direct Resolution self-consistent potential corresponding to the time iteration l of Algorithm 4.1. Is also given the corresponding total number of iterations l_{tot}, the CPU time of the method and the *Final dist* which corresponds to the value of the quantity (5.1) for $l = l_{tot}$.
In the first graphic of Figure 5, the number of frequency points is $P = 3750$ and we use the boundary conditions (C.9)(C.12) for the time-dependent Schrödinger equation where the angular frequencies are given by (C.13)(C.14). When the extrapolation of the intermediary potential $V^{l+\frac{1}{2}}$ is given by (4.3), curve title Pinaud, the Direct Resolution verifies the convergence criterion to the stationary potential V_∞ only for the time step $\Delta t = 10^{-15}s$. Although $\Delta t = 2 \times 10^{-15}s$ verifies the Schrödinger equation time step limit (4.2), the method is clearly unstable for this time step

and the loss of stability comes from (4.3). When the extrapolation is given by (4.4), curve title ABCN, the Direct Resolution potential convergences to V_∞ for both time steps $\Delta t = 10^{-15}s$ and $\Delta t = 2 \times 10^{-15}s$ and the CPU time is reduced for the second time step. However the increase of the time step makes the amplitude of the transient oscillations of the potential slightly bigger.
In the second graphic of Figure 5, the number of frequency points is $P = 3750$ and we use the boundary conditions (C.9)(C.12) and the extrapolation (4.4) for the intermediary potential $V^{l+\frac{1}{2}}$. When the angular frequencies are the discrete ones (C.13)(C.14), curve title Disc AF, the Direct Resolution potential convergences to V_∞ and *Final dist* is small enough for both time steps $\Delta t = 10^{-15}s$ and $\Delta t = 2 \times 10^{-15}s$. When the angular frequencies are the continuous ones (C.8)(C.11), curve title Cont AF, no instability is noticed, however, the value *Final dist* is bigger than the value given in Disc AF and increases with the time step. In the case Disc AF, the computational cost is largely reduced with a good enough accuracy using the simplified boundary conditions (C.21)(C.22) for $l \geq M + 2$ and $M = 500$, curve title Disc AF-$M = 500$. Indeed, the CPU time is divided by more than two for $\Delta t = 10^{-15}s$ and, for the two time steps considered, the value *Final dist* is less than 10^{-2}.
In the third graphic of Figure 5, we use the boundary conditions (C.9)(C.12) where the angular frequencies are given by (C.13)(C.14) and the extrapolation (4.4) for the intermediary potential $V^{l+\frac{1}{2}}$. The different curves correspond to different values of the parameter P, curve title $P = 3750$, $P = 2100$ and $P = 450$. The case $P = 2100$ illustrates the fact that a reasonable accuracy is obtained for big enough number of frequency points under the limit $P = 3700$ of sure convergence of the stationary method. This fact is relatively stable with respect to the time step and allows a reduction of the CPU time of the method. However, the number of frequency points can not be chosen too small: in the case $P = 450$, the value *Final dist* is bigger than 10^{-1} and the amplitude of the transient oscillations of the potential are large compared to the case $P = 3750$. As in the stationary case, a big number of frequency points, and therefore a relatively hight numerical cost, is required for the Direct Resolution, which enhances the importance of our alternative method.

5.3.2 The One Mode Approximation

Before comparing the two methods presented in section 4, we show how the parameters of the One Mode Approximation method have to be adjusted, as we did in section 5.3.1 for the Direct Resolution.
The initial data of the method is given by the stationary One Mode Approximation for the initial bias $B_I = 0\,eV$ and the parameters given in section 5.2 where $P = 3900$ and $P' = 300$. The stationary potential V_∞ corresponding to B_∞ is computed in the same way.
For different parameters of the method, is represented in Figure 6 the time evolution of the l^2-norm relative distance (5.1) to the potential V_∞ where V^l is the One Mode Approximation self-consistent potential corresponding to the time iteration l of Algorithm 4.1. As in section 5.3.1, is given the corresponding total number of iterations l_{tot}, the CPU time of the method and the number *Final dist*. For all the curves represented, the time-dependent Schrödinger equation boundary conditions are given by (C.9)(C.12), the angular frequencies by (C.13)(C.14) and the extrapolation of the intermediary potential by (4.4). The number of frequency points corresponding to the thin mesh is equal to $P = 3900$.
In the first graphic of Figure 6, the number of frequency points corresponding to the coarse mesh is equal to $P' = 300$. When the angular frequency ω_p^∞ in (4.22) is the discrete one (4.24), curve title Oscill Interpolation, the One Mode Approximation verifies the convergence criterion to the stationary potential V_∞ for both time steps $\Delta t = 10^{-15}s$ and $\Delta t = 2 \times 10^{-15}s$. This is also true when the angular frequency ω_p^∞ is the continuous one (4.23), curve title Oscill Interpolation-Cont AF. However, in the case Oscill Interpolation, the value *Final dist* is smaller and the method provides a more accurate solution. In the last case, the CPU time is largely reduced while conserving a correct accuracy, and the stability with respect to the time step, compared to the results provided by the Direct Resolution in section 5.3.1. The constant interpolation of the non resonant wave function, curve title Const Interpolation, is obtained by taking the angular frequency ω_p^∞ equal to 0 in (4.22). In that case, the One Mode Approximation is not accurate: the value *Final dist* is

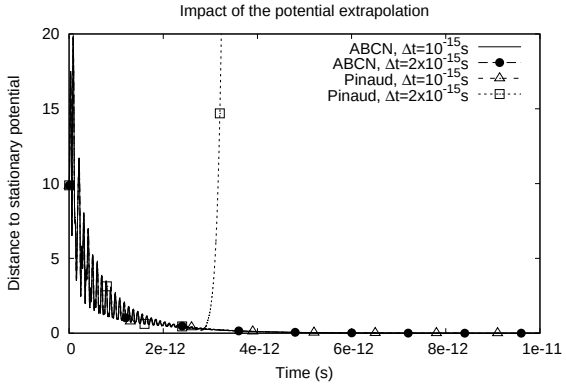

	l_{tot}	CPU(s)	Final dist (%)
ABCN, $\Delta t = 10^{-15}\ s$	10^4	3880.4	4.4598×10^{-4}
ABCN, $\Delta t = 2 \times 10^{-15}\ s$	5×10^3	1387.0	6.0283×10^{-4}
Pinaud, $\Delta t = 10^{-15}\ s$	10^4	3864.8	4.4609×10^{-4}
Pinaud, $\Delta t = 2 \times 10^{-15}\ s$	5×10^3	1440.7	353.28

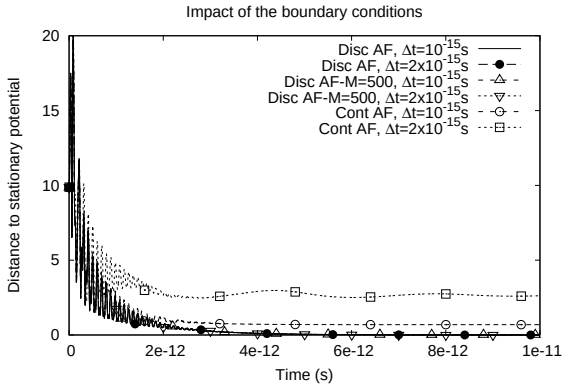

	l_{tot}	CPU(s)	Final dist (%)
Disc AF, $\Delta t = 10^{-15}\ s$	10^4	3880.4	4.4598×10^{-4}
Disc AF, $\Delta t = 2 \times 10^{-15}\ s$	5×10^3	1387.0	6.0283×10^{-4}
Disc AF-$M = 500$, $\Delta t = 10^{-15}\ s$	10^4	1830.4	8.0349×10^{-3}
Disc AF-$M = 500$, $\Delta t = 2 \times 10^{-15}\ s$	5×10^3	916.06	4.5206×10^{-3}
Cont AF, $\Delta t = 10^{-15}\ s$	10^4	3867.8	0.6874
Cont AF, $\Delta t = 2 \times 10^{-15}\ s$	5×10^3	1388.1	2.6214

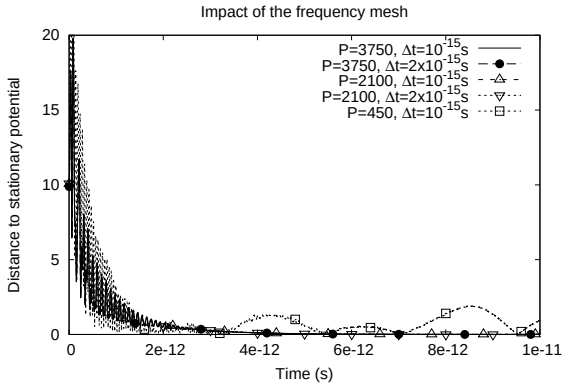

	l_{tot}	CPU(s)	Final dist (%)
$P = 3750$, $\Delta t = 10^{-15}\ s$	10^4	3880.4	4.4598×10^{-4}
$P = 3750$, $\Delta t = 2 \times 10^{-15}\ s$	5×10^3	1387.0	6.0283×10^{-4}
$P = 2100$, $\Delta t = 10^{-15}\ s$	10^4	2252.7	9.7708×10^{-3}
$P = 2100$, $\Delta t = 2 \times 10^{-15}\ s$	5×10^3	874.72	4.5743×10^{-3}
$P = 450$, $\Delta t = 10^{-15}\ s$	10^4	636.82	0.94840

Figure 5: Evolution of the potential relative distance (5.1) to the stationary solution for the Direct Resolution. From top to bottom: Impact of the potential extrapolation, Impact of the boundary conditions and Impact of the frequency mesh.

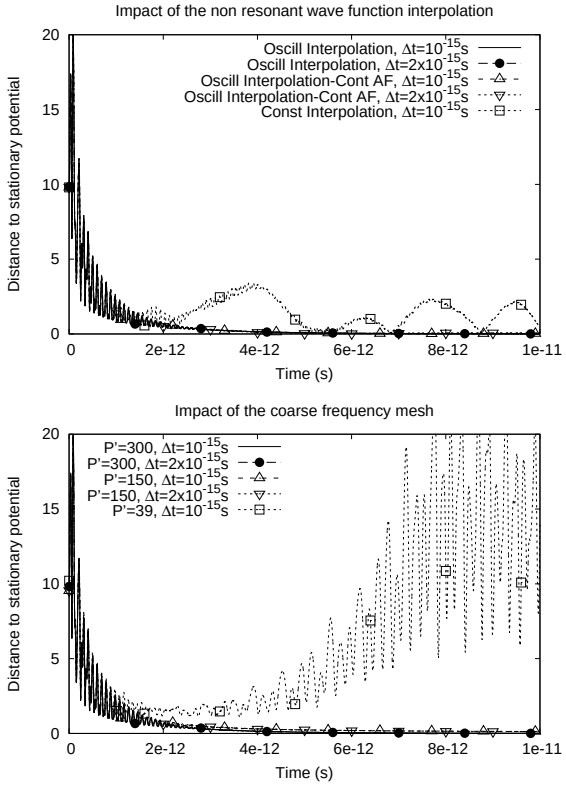

	l_{tot}	CPU(s)	Final dist (%)
Oscill Interpolation, $\Delta t = 10^{-15}\ s$	10^4	496.03	5.5306×10^{-3}
Oscill Interpolation, $\Delta t = 2 \times 10^{-15}\ s$	5×10^3	204.29	6.4993×10^{-3}
Oscill Interpolation- Cont AF, $\Delta t = 10^{-15}\ s$	10^4	497.31	2.1769×10^{-2}
Oscill Interpolation- Cont AF, $\Delta t = 2 \times 10^{-15}\ s$	5×10^3	206.05	7.7645×10^{-2}
Const Interpolation $\Delta t = 10^{-15}\ s$	10^4	506.45	0.42549

	l_{tot}	CPU(s)	Final dist (%)
$P' = 300$, $\Delta t = 10^{-15}\ s$	10^4	496.03	5.5306×10^{-3}
$P' = 300$, $\Delta t = 2 \times 10^{-15}\ s$	5×10^3	204.29	6.4993×10^{-3}
$P' = 150$, $\Delta t = 10^{-15}\ s$	10^4	344.06	0.12238
$P' = 150$, $\Delta t = 2 \times 10^{-15}\ s$	5×10^3	152.50	0.12444
$P' = 39$, $\Delta t = 10^{-15}\ s$	10^4	242.87	14.176

Figure 6: Evolution of the potential relative distance (5.1) to the stationary solution for the One Mode Approximation. From top to bottom: Impact of the interpolation of the non resonant wave function and Impact of the coarse frequency mesh.

bigger than 10^{-1} and the potential oscillates when the time t is bigger that $2 \times 10^{-12}s$.
In the second graphic of Figure 6, the angular frequency ω_p^∞ is given by (4.24). The different curves correspond to different values of the parameter P', curve title $P' = 300$, $P' = 150$ and $P' = 39$. The case $P' = 150$ illustrates the fact that the CPU time can be reduced by reducing the number P' of Schrödinger equations to be solved and allowing a lower, but still reasonable, accuracy. This fact is relatively stable with respect to the time step. However, it is clear from the case $P' = 39$ that P' can not be too small.

As in the Direct Resolution, the extrapolation equation (4.4) and the discrete angular frequencies (C.13)(C.14) present an improvement compared to the extrapolation equation (4.3) and the angular frequencies (C.8)(C.11). Here also, the CPU time can be reduced within a reasonable range of accuracy by using the simplified boundary conditions (C.21)(C.22) or by taking the number of frequency points, of the thin mesh, big enough below the limit $P = 3700$.

5.3.3 Comparison for a suitable fixed set of parameters

We consider now Figure 7 and Table 2 where is given a numerical comparison of the methods presented in section 4: the Direct Resolution and One Mode Approximation. The Direct Resolution plays the role of the reference method.
For the Direct Resolution, resp. One Mode Approximation, the initial data of the method and the stationary potential V_∞ and density n_∞ corresponding to the final bias B_∞ are obtained as in section 5.3.1, resp. 5.3.2, where $P = 3900$ and $P' = 300$.
For the two methods, the time-dependent Schrödinger equation boundary conditions are given by (C.21)(C.22) with $M = 500$, the corresponding angular frequencies by (C.13)(C.14) and the

	CPU(s)	Final dist (%)
Direct	952.35	4.4593×10^{-3}
One Mode	159.30	1.0857×10^{-2}

Table 2: Comparison of the Direct Resolution and One Mode Approximation for the resolution of the time-dependent Schrödinger-Poisson system (2.1)(2.2)(2.3) for $M = 500$, $P = 3900$, $P' = 300$, $\Delta t = 2 \times 10^{-15}\, s$ and $l_{tot} = 5 \times 10^3$.

extrapolation of the intermediary potential by (4.4). The frequency mesh is given by the integers $P = 3900$ and $P' = 300$, the total number of iterations is equal to $l_{tot} = 5 \times 10^3$ and the time step is equal to $\Delta t = 2 \times 10^{-15}\, s$. The last verifies the condition (4.2). For the One Mode Approximation the angular frequency ω_p^∞ is given by (4.24).
In the graphic of Figure 7 entitled *Convergence to stationary density*, is represented the time evolution of the l^2-norm relative distance to the density n_∞:

$$100 \frac{|n^l - n_\infty|_2}{|n_\infty - n_D|_2} \tag{5.2}$$

where n^l is the electron density corresponding to the time iteration l of Algorithm 4.1. The relevant variation of the density being in the device, interval (a_1, b_1), we considered in (5.2) the relative distance from $(n^l - n_D)$ to $(n_\infty - n_D)$. In the graphic entitled *Evolution of the resonant energy*, is represented the time evolution of the real part of the first resonance z^l computed using the method presented in section 3.2 where the potential Q is equal to $U^l + V^l$. In the two last graphics of Figure 7, together with the Direct Resolution self-consistent potential (resp. probability density) at final time step, curve title Direct, is represented the stationary Direct Resolution potential V_∞ (resp. density n_∞), curve title Direct-V_∞ (resp. Direct-n_∞). The same was done for the One Mode Approximation: curve title One Mode, One Mode-V_∞, One Mode-n_∞. In Table 2, the column CPU denotes the CPU time of the method and the column *Final dist* is the value of the quantity (5.1) for $l = l_{tot}$.
The two methods behave the same qualitatively: the potential (resp. density) converges, up to a small error, to V_∞ (resp. n_∞). At time $t = 0^+$, the current is close to the current corresponding to B_I. This is not true for the energy due to the discontinuity of the bias at $t = 0$ and the fact that the self-consistent potential is small compared to the external potential. After fast transient oscillations, the current stabilize in a short time to a value relatively close to the current corresponding to B_∞ compared to the total variation of the current on the interval $t \geq 0$. Differently, the energy continues to increase slowly to such a value after the slightly longer transient oscillations. The comparison is also favorable quantitatively. Indeed, at each time step, the currents provided by the two methods are relatively close of each other compared to the total variation of the current on the interval $t \geq 0$, therefore, the One Mode Approximation wave functions are computed accurately in comparison with the Direct Resolution. Similarly, at each time step, the small relative difference between the energies provided by the two methods validates the One Mode Approximation self-consistent potential in comparison with the Direct Resolution. We conclude that for the parameters (of the two methods) chosen in this section, the One Mode Approximation provides a solution accurate enough at each time step with a reduction of the CPU time by a factor close to 6 compared to the Direct Resolution.

The above comparison was not performed with the parameters of the reference method which give the best accuracy/CPU time ratio. However, the alternative method provides an effective improvement. Indeed, when the parameters of the Direct Resolution are adjusted, as explained in section 5.3.1, to reduce the CPU time within a reasonable range of accuracy, the One Mode Approximation with suitable parameters provides a solution in the same range of accuracy for a lower CPU time.

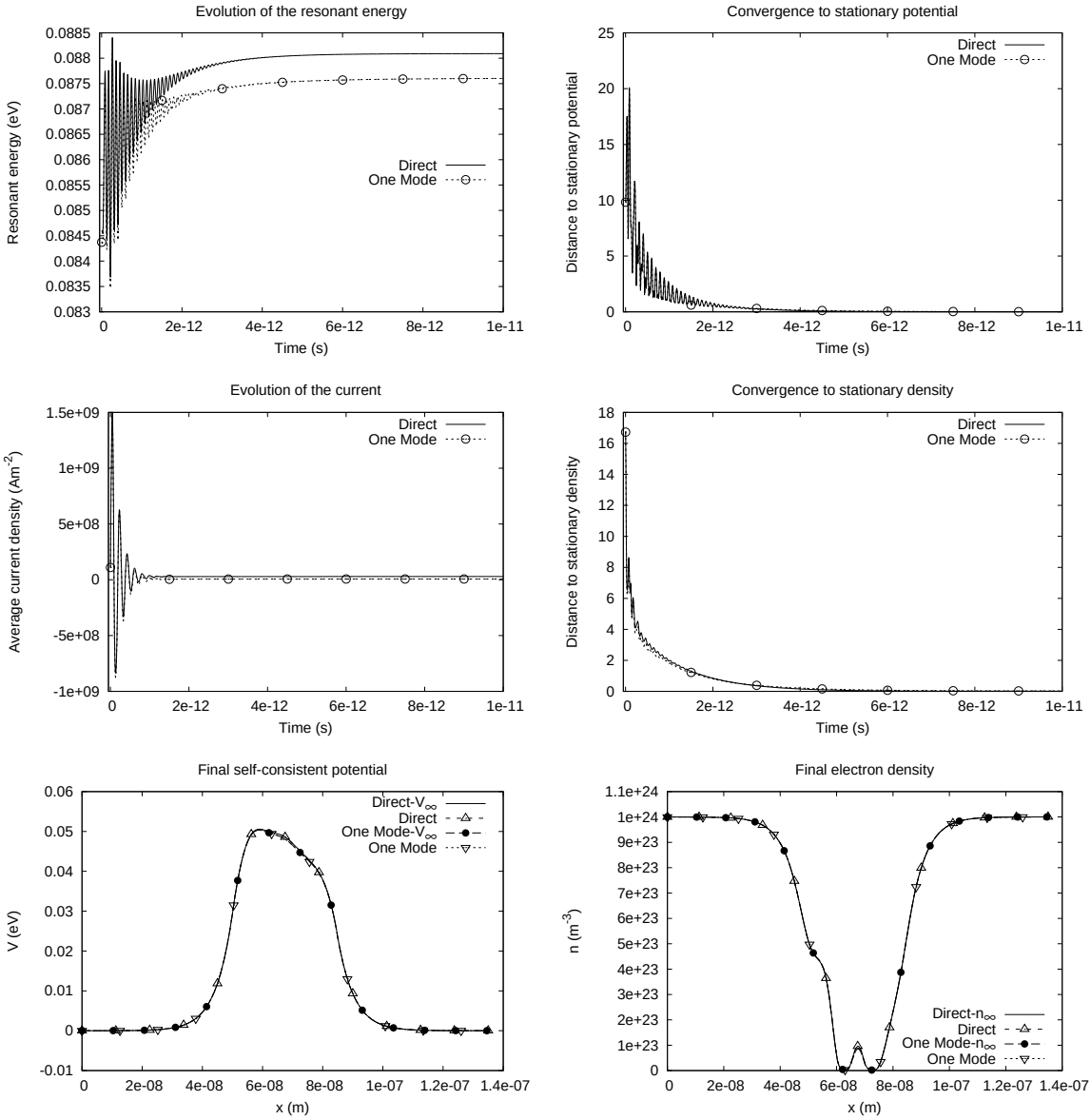

Figure 7: For $M = 500$, $P = 3900$, $P' = 300$, $\Delta t = 2 \times 10^{-15}\, s$, $l_{tot} = 5 \times 10^3$ and, for the methods considered, are represented from left to right: Evolution of the real part of the first resonance (resonant energy), Evolution of the potential relative distance (5.1) to the stationary solution, Evolution of the average current density defined by (5.3), Evolution of the density relative distance (5.2) to the stationary solution, Self-consistent potential at final iteration l_{tot}, and Electron density at final iteration l_{tot}.

Remark 5.2. As it is proposed in [12], the average current density at time t is defined by:

$$\mathcal{J}(t) = \frac{q\hbar}{m}\int_{I\!R} g(k)\mathrm{Im}\left[\frac{1}{L}\int_0^L \partial_x\Psi_k(t,x)\overline{\Psi_k(t,x)}dx\right]dk \tag{5.3}$$

In (5.3), the space derivative is computed using the finite difference method. For the Direct Resolution, the integral with respect to the frequency k is computed using the trapezoidal rule with the frequency mesh we used to compute the density. For the One Mode Approximation, the frequency integral is given by a double scale trapezoidal rule of the form (4.21). As we did for the density, it is obtained by injecting in (5.3) the decomposition (4.14) of the wave function and neglecting the cross term between the resonant and the non resonant part.

5.3.4 Time evolution of the electron repartition with respect to the frequency

For biases of the form (4.1), since the change of potential at time $t = 0$ is abrupt, the adiabaticity hypothesis of [40] is not satisfied and one expects two peaks corresponding to both the resonant energy at time $t = 0^-$ and the resonant energy at time t. This is what we show numerically using the Direct Resolution and the One Mode Approximation.
The parameters and the initialization of the two methods are the same than in section 5.3.3. Since we are not looking at the CPU time, we took however the complete Schrödinger equation boundary conditions (C.9)(C.12) instead of (C.21)(C.22) and the time step equal to $\Delta t = 10^{-15}\,s$ instead of $\Delta t = 2\times 10^{-15}\,s$.
In Figure 8, for the curve with title Direct, the number of electrons in the island corresponding to one wave function is given by:

$$N^l_{di,p} = \sum_{j\in w_{is}} |\Psi^l_{p,j}|^2\Delta x \tag{5.4}$$

where $\Psi^l_{p,j}$ is the Direct Resolution wave function defined in section 4.1 and $w_{is} = \{j\,|\,a_2 \le x_j < b_2\}$. For the curve with title One Mode, the cross term between the resonant and the non resonant part of the wave function is neglected and equation (5.4) becomes:

$$N^l_{om,p} = \sum_{j\in w_{is}} \left|\Psi^{nr,l}_{p',j}\right|^2\Delta x + \left|\lambda^l_p\right|^2\sum_{j\in w_{is}}\left|u_j^{l-\frac{1}{2}}\right|^2\Delta x \tag{5.5}$$

where $\Psi^{nr,l}_{p',j}$, λ^l_p and $u_j^{l-\frac{1}{2}}$ are the components, defined in section 4.2.2, of the One Mode Approximation wave function. As in section 4.2.2, $0 \le p' \le P'$ is the integer such that $p = \nu p' + r$ for some $0 \le r \le \nu - 1$, in other terms, we made in (5.5) a constant interpolation of the non resonant wave function for $p \ne \nu p'$. Consider the numbers $E^l \in I\!R$ and $\Gamma^l > 0$ such that

$$z^l = E^l - i\Gamma^l$$

where z^l is the Direct Resolution resonance, at time t^l, defined in section 5.3.3. Then, the resonant frequencies

$$k^l_- = -\sqrt{\frac{2m}{\hbar^2}\left(E^l + B_\infty\right)}\,, \qquad k^l_+ = \sqrt{\frac{2m}{\hbar^2}E^l}\,, \tag{5.6}$$

are the real numbers related to the resonant energy E^l according to the relation (4.13).
We can now discuss the results in Figure 8. For the Direct Resolution, we observe that for small times t^l, the localization of the resonance peak is not given by the resonant energy E^l but by the resonant energy at time $t = 0^-$: E_I. Indeed, for such times, the number of electrons $N^l_{di,p}$ defined in (5.4) has only one peak which is located at the frequencies such that $E_k = E_I$ where E_k and E_I are given by (2.8) and (3.20) (The numerical value of E_I is computed as in section 5.1 where $B_I = 0\,eV$ and $P = 3900$). When time goes, the first peak persists but decays slowly while a second peak appears and then grows at the frequencies k^l_- and k^l_+ defined in (5.6). Using the definition of k^l_- and k^l_+, the last statement means that the second peak lives at the frequencies

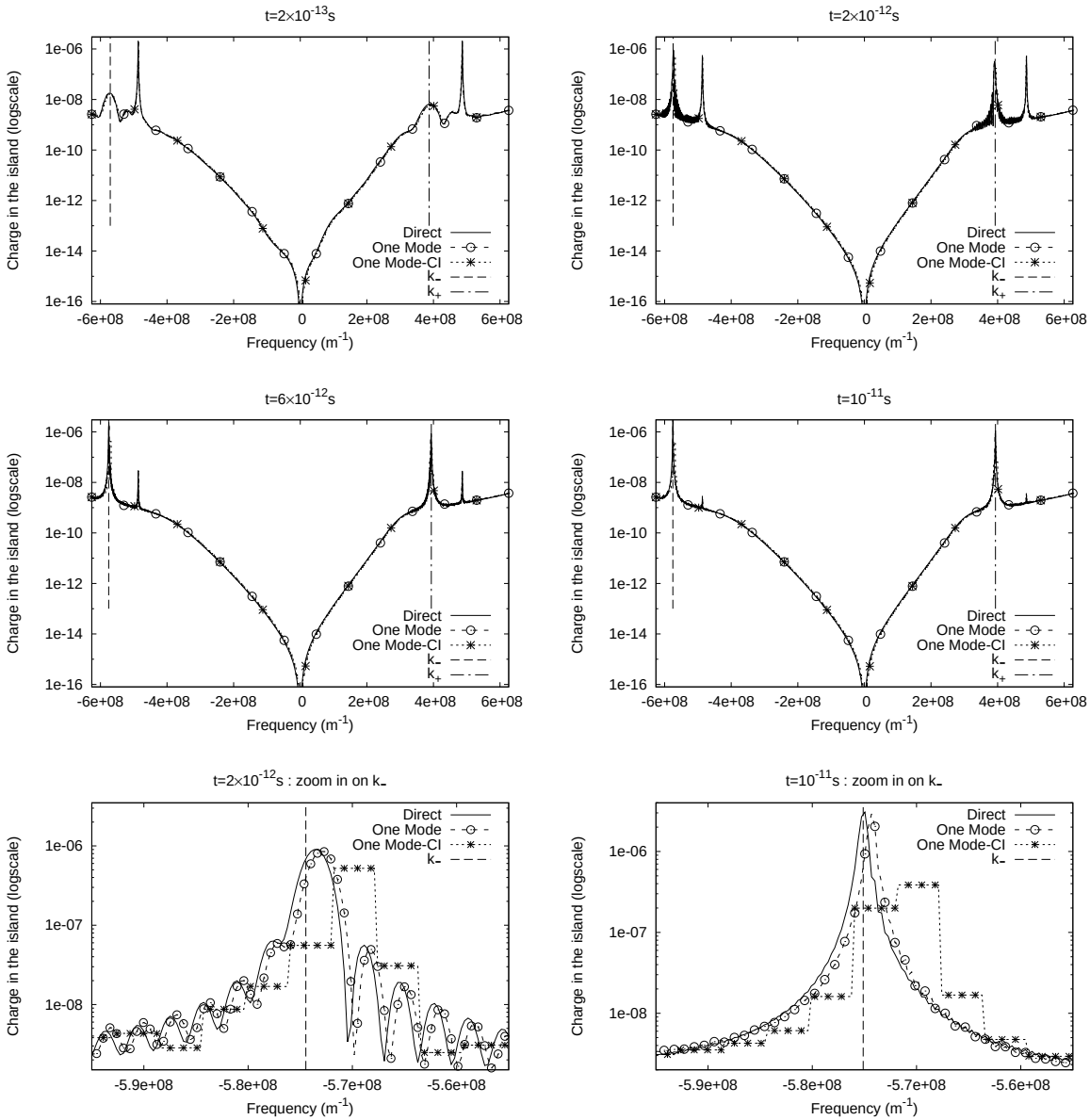

Figure 8: For $P = 3900$, $P' = 300$, $\Delta t = 10^{-15}\, s$ and at different values of the time t: Number (5.4) of electrons in the island for one wave function with respect to the frequency k for the Direct Resolution, Number (5.5) of electrons in the island for one wave function with respect to the frequency k for the One Mode Approximation, and Resonant frequencies given by (5.6) (a vertical line is represented at these frequencies). Is represented a zoom in on k_-^l of the above curves at time $t = 2 \times 10^{-12}\, s$ and $t = 10^{-11}\, s$.

such that $\varepsilon_k^\infty = E^l$. At time $t^l = 10^{-11}\,s$, the initial peak has almost vanished and the second peak almost reached its maximal amplitude.
For the One Mode Approximation, the first peak is provided by the initial condition and, as stated in section 4.2.2, the accuracy of the second peak is reached only if the interpolation of the non resonant wave function in (4.16) is well chosen. In particular, the constant interpolation computed as explained in section 5.3.2, curve title One Mode-CI, provides a piecewise constant function close to the resonant frequencies k_-^l and k_+^l and therefore does not describe correctly the second peak (this is clear in the two last graphics of Figure 8). Whereas in the case of the oscillatory interpolation, which corresponds to the iteration (4.22), the coefficient λ_p^l is such that, for large times, the number of electrons $N_{om,p}^l$ defined in (5.5) has a sharp peak at the frequencies k_-^l and k_+^l with amplitude high enough and the One Mode Approximation is accurate compared to the Direct Resolution.

Acknowledgements. The authors acknowledge support from the project QUATRAIN (BLAN07-2

212988) funded by the French Agence Nationale de la Recherche and from the Marie Curie Project DEASE: MEST-CT-2005-021122 funded by the European Union. The second author acknowledges Prof. Norbert Mauser for his hospitality in WPI Vienna where a part of the present work was achieved.

A Resolution of the stationary Schrödinger equation using finite difference

Discrete transparent boundary conditions are proposed in [3] to solve equation (2.5) on the domain $[0, L]$ using finite difference. In order to be able to justify the choice of the transparent boundary conditions in section B, we recall how the method follows under the assumption $k > 0$ in [3] and we give an extension of this method to the case $k < 0$.
For a given potential Q_I such that:

$$Q_I(x) = 0,\ x \leq 0, \quad \text{and} \quad Q_I(x) = Q_{I,L},\ x \geq L\,, \tag{A.1}$$

and a given wave vector $k \in I\!R$, we consider the stationary Schrödinger equation

$$-\frac{\hbar^2}{2m}\partial_x^2\Phi + Q_I\Phi = E_k\Phi, \quad x \in I\!R \tag{A.2}$$

with the k-dependent scattering conditions (2.6), (2.7).
Using the space discretization defined in section 3.1 and noting Φ_j the approximation of the wave function $\Phi(x_j)$ and $Q_{I,j}$ the approximation of the potential $Q_I(x_j)$, the finite difference method for equation (A.2) writes:

$$D_x^2\Phi_j = \frac{2m}{\hbar^2}(Q_{I,j} - E_k)\Phi_j, \quad j = 1, ..., J-1 \tag{A.3}$$

where

$$D_x^2\Phi_j = \frac{\Phi_{j+1} - 2\Phi_j + \Phi_{j-1}}{\Delta x^2}$$

For $k > 0$, the energy is given by $E_k = \frac{\hbar^2 k^2}{2m}$. Then, thanks to assumption (A.1), the solutions to equation (A.3) can be computed explicitly for $j \leq 1$. Indeed, under the condition

$$\Delta x < \frac{1}{\sqrt{k^2 + \frac{2m}{\hbar^2}|Q_{I,L}|}}\,, \tag{A.4}$$

they correspond to the linear combinations of α_1^j, α_2^j where:

$$\alpha_{1,2} = 1 - \Delta x^2\frac{k^2}{2} \pm i\sqrt{\Delta x^2 k^2 - \Delta x^4\frac{k^4}{4}} \tag{A.5}$$

are complex numbers verifying $|\alpha_j| = 1$ and $\alpha_1 = e^{i\tilde{k}\Delta x}$ for some $\tilde{k} > 0$. Then α_1^j is an incoming plane wave, $\alpha_2^j = \alpha_1^{-j}$ is the reflected wave and the discrete analogous to the scattering condition (2.6) is to select the linear combinations of α_1^j, α_2^j of the form:

$$\Phi_j = \alpha_1^j + R\alpha_1^{-j}, \quad j \leq 1 \tag{A.6}$$

Applying equation (A.6) to compute Φ_0 and Φ_1, we get the following discrete transparent boundary condition at $x = 0$:

$$\alpha_1^{-1}\Phi_0 - \Phi_1 = \alpha_1^{-1} - \alpha_1 \tag{A.7}$$

We note that the inequality (A.4) implies $\tilde{k}\Delta x < \frac{\pi}{2}$ and the discretization provides enough space points in one wave length of the discrete plane wave.
Similarly, for $j \geq J$ it holds $Q_{I,j} = Q_{I,L}$ and, if $k^2 - \frac{2m}{\hbar^2}Q_{I,L} > 0$, the solutions to equation (A.3) are the linear combinations of β_1^j, β_2^j where:

$$\beta_{1,2} = 1 - \Delta x^2(\frac{k^2}{2} - \frac{m}{\hbar^2}Q_{I,L}) \pm i\sqrt{\Delta x^2(k^2 - \frac{2m}{\hbar^2}Q_{I,L}) - \Delta x^4(\frac{k^2}{2} - \frac{m}{\hbar^2}Q_{I,L})^2} \tag{A.8}$$

Inequality (A.4) implies $|\beta_j| = 1$ and $\beta_1 = e^{i\tilde{k}\Delta x}$ for some $\tilde{k} > 0$. Then β_1^j is an outgoing wave and the scattering condition (2.6) gives:

$$\Phi_j = T\beta_1^j, \quad j \geq J - 1 \tag{A.9}$$

Applying equation (A.9) to compute Φ_{J-1} and Φ_J, we get the following discrete transparent boundary condition at $x = L$:

$$-\Phi_{J-1} + \beta_1^{-1}\Phi_J = 0 \tag{A.10}$$

Again, condition (A.4) implies $\tilde{k}\Delta x < \frac{\pi}{2}$. If $k^2 - \frac{2m}{\hbar^2}Q_{I,L} \leq 0$, the bounded solutions to (A.3) for $j \geq J - 1$ are given by (A.9), where Φ_j is constant in the case of the equality and vanishing in the case of the strict inequality, and (A.10) still apply.
For $k < 0$, the energy is given by $E_k = \frac{\hbar^2 k^2}{2m} + Q_{I,L}$. Then, using the assumptions (A.1), (A.4) and repeating the above calculations where the scattering condition (2.6) is replaced by (2.7), we obtain the following transparent boundary conditions for equation (A.3) at $x = 0$ and $x = L$:

$$\beta_2\Phi_0 - \Phi_1 = 0 \tag{A.11}$$

$$-\Phi_{J-1} + \alpha_2\Phi_J = \alpha_2^J(\alpha_2 - \alpha_2^{-1}) \tag{A.12}$$

where α_2 is given by equation (A.5) and

$$\beta_{1,2} = 1 - \Delta x^2(\frac{k^2}{2} + \frac{m}{\hbar^2}Q_{I,L}) \pm i\sqrt{\Delta x^2(k^2 + \frac{2m}{\hbar^2}Q_{I,L}) - \Delta x^4(\frac{k^2}{2} + \frac{m}{\hbar^2}Q_{I,L})^2} \tag{A.13}$$

For $k > 0$, the scheme (A.3) with the boundary conditions (A.7)(A.10) has a unique solution. By construction, the unique solution Φ_j to the whole-space scheme (A.3) considered on $j \in \mathbb{Z}$ with the scattering conditions (A.6)(A.9) verifies the problem (A.3)(A.7)(A.10). It follows that the solution to (A.3)(A.7)(A.10) corresponds exactly with the restriction of Φ_j to $0 \leq j \leq J$. A similar property is true for $k < 0$. Moreover we have the following estimate on the solution:

Lemma A.1. *There exists a constant $C > 0$ which depends only on $\hbar$, m, L, $Q_{I,L}$, $\sup_{x\in(0,L)} |Q_I(x)|$, k such that for all Δx verifying* (A.4)*, the solution to the scheme* (A.3) *with the boundary conditions* (A.7)(A.10) *for $k > 0$ and* (A.11)(A.12) *for $k < 0$ verifies:*

$$\|\Phi\|_2 \leq C$$

where

$$\|\Phi\|_2^2 = \sum_{j=1}^{J-1} |\Phi_j|^2 \Delta x$$

B Computation of resonances using finite difference

For a given potential Q verifying (3.5), we give in this section a discrete version of the following problem: find (u, z) solution to (3.7) such that u is purely outgoing outside the interval $[0, L]$.
Using the decay at infinity of the function g in (2.4), it follows that only the resonances with real part smaller than $\frac{\hbar^2\kappa^2}{2m}$ are important for the computation of the density, where κ is defined in section 3.1. Then, if we suppose that the resonances have positive real part, which is no real restriction in applications, the problem of the computation of resonances can be written for z in the strip

$$S = \left\{ z \in \mathbb{C} \,|\, 0 < \mathrm{Re}\,(z) < \frac{\hbar^2\kappa^2}{2m} \right\}$$

In order to work with analytic functions on S, the value of the square root function $\sqrt{z}$ will be the principal value.
Proceeding as in section A, we write first the finite difference method for equation (3.7):

$$D_x^2 u_j = \frac{2m}{\hbar^2}(Q_j - z)u_j, \quad j = 1, ..., J-1 \tag{B.1}$$

where u_j denotes the approximation of the resonant mode $u(x_j)$ and Q_j the approximation of the potential $Q(x_j)$. Thanks to assumption (3.5), the solutions to equation (B.1) can be computed explicitly for $j \leq 1$. Indeed, under the condition

$$\Delta x < \frac{1}{\sqrt{\kappa^2 + \frac{2m}{\hbar^2}|Q_L|}} \tag{B.2}$$

they correspond to the linear combinations of $\alpha_1(z)^j$, $\alpha_2(z)^j$ where:

$$\alpha_{1,2}(z) = 1 - \Delta x^2 \frac{m}{\hbar^2} z \pm i\sqrt{2\Delta x^2 \frac{m}{\hbar^2} z - \Delta x^4 \frac{m^2}{\hbar^4} z^2} \tag{B.3}$$

Utilizing the forthcoming equation (B.11), it holds $\alpha_2(z) = \rho e^{ik\Delta x}$ with $\rho > 0$ and $k < 0$. Since we are looking for solutions which are outgoing outside $[0, L]$, we impose:

$$u_j = R\alpha_2(z)^j, \quad j \leq 1 \tag{B.4}$$

Applying equation (B.4) to compute u_0 and u_1, we get the following discrete transparent boundary condition at $x = 0$:

$$\alpha_2(z)u_0 - u_1 = 0 \tag{B.5}$$

Similarly, for $j \geq J$ it holds $Q_j = Q_L$ and the solutions to equation (B.1) are the linear combinations of $\beta_1(z)^j$, $\beta_2(z)^j$ where:

$$\beta_{1,2}(z) = 1 - \Delta x^2 \frac{m}{\hbar^2}(z - Q_L) \pm i\sqrt{2\Delta x^2 \frac{m}{\hbar^2}(z - Q_L) - \Delta x^4 \frac{m^2}{\hbar^4}(z - Q_L)^2} \tag{B.6}$$

Using equation (B.11), the outgoing wave is identified with the plus sign in (B.6), therefore we impose:

$$u_j = T\beta_1(z)^j, \quad j \geq J-1 \tag{B.7}$$

Applying equation (B.7) to compute u_{J-1} and u_J, we get the following discrete transparent boundary condition at $x = L$:

$$-u_{J-1} + \beta_1(z)^{-1}u_J = 0$$

Since $\beta_1(z)\beta_2(z) = 1$, the previous equation writes:

$$-u_{J-1} + \beta_2(z)u_J = 0 \tag{B.8}$$

In order to work with quantities of order 1, the condition $u^H u = 1$ is imposed instead of the norm condition in (3.7) and the resonant mode have to be multiplied by $\Delta x^{\frac{1}{2}}$ to verify $\sum_{j=0}^{J} |u_j|^2 \Delta x = 1$. Then, it follows from equations (B.1), (B.5) and (B.8) that the sought discrete problem is

$$\begin{cases} M(z)u = 0 \\ u^H u = 1 \end{cases} \tag{B.9}$$

where

$$M(z) = \begin{pmatrix} \alpha_2(z) & -1 & & & & \\ -1 & 2 + \frac{2m\Delta x^2}{\hbar^2}(Q_1 - z) & -1 & & & 0 \\ & \ddots & \ddots & & \ddots & \\ & & -1 & 2 + \frac{2m\Delta x^2}{\hbar^2}(Q_{J-1} - z) & -1 & \\ 0 & & & -1 & \beta_2(z) & \end{pmatrix} \tag{B.10}$$

We note that, in S, the holomorphy of $M(z)$ required in section 3.2 is verified.
We now give an interpretation of the solutions to the problem (B.9). In the strip S, resonances can be defined at the discrete level as the complex numbers z such that the whole-space scheme (B.1) considered on $j \in \mathbb{Z}$ has purely outgoing solutions, i.e. solutions verifying (B.4) and (B.7). When z is a resonance, such a solution is a called a resonant mode and it is uniquely determined up to a phase factor. Moreover, it holds that a complex number z is a resonance if and only if z is such that there exists a vector u verifying (B.9). This implies that if z is a resonance, the corresponding u solution to (B.9) is equal to the restriction of the resonant mode to $0 \leq j \leq J$ (up to a phase factor again).

Proposition B.1. *If Δx verifies the condition* (B.2)*, then for all z in S the coefficients defined in* (B.3) *and* (B.6) *verify*

$$Im(\alpha_1(z)) > 0\,, \quad Im(\alpha_2(z)) < 0 \quad \textit{and} \quad Im(\beta_1(z)) > 0\,, \quad Im(\beta_2(z)) < 0 \tag{B.11}$$

If moreover $Im(z) < 0$, it holds

$$|\alpha_1(z)| > 1\,, \quad |\alpha_2(z)| < 1 \quad \textit{and} \quad |\beta_1(z)| > 1\,, \quad |\beta_2(z)| < 1$$

In the next proposition, we show that resonances have negative imaginary part. This, combined with Proposition B.1 and equations (B.4)(B.7), implies that the corresponding resonant modes tend to the infinity when $j \to \pm\infty$. It is the discrete transcription of the fact that the space $L^2(\mathbb{R})$ has to be deformed in order to consider resonances as eigenvalues.

Proposition B.2. *If Δx verifies the condition* (B.2)*, then if $z \in S$ is such that the problem* (B.9) *has a solution u, it holds $Im(z) < 0$.*

Proof. We multiply equation (B.1) by $\overline{u_j}$ and sum up for $j = 1, ..., J-1$. Then, utilizing the summation by part rule:

$$\sum_{j=1}^{J-1} g_j D_x^- f_j = -\sum_{j=0}^{J-1} f_j D_x^+ g_j + \frac{1}{\Delta x}(f_{J-1} g_J - f_0 g_0) \tag{B.12}$$

where

$$D_x^+ f_j = \frac{f_{j+1} - f_j}{\Delta x}, \quad D_x^- f_j = \frac{f_j - f_{j-1}}{\Delta x}, \quad D_x^- D_x^+ f_j = D_x^2 f_j$$

we get

$$\sum_{j=0}^{J-1} \left|D_x^+ u_j\right|^2 = -\sum_{j=1}^{J-1} \frac{2m}{\hbar^2}(Q_j - z)|u_j|^2 + \frac{1}{\Delta x}\left(D_x^+ u_{J-1}\overline{u_J} - D_x^+ u_0 \overline{u_0}\right) \tag{B.13}$$

Applying the boundary conditions (B.5)(B.8) in (B.13) and taking the imaginary part, it follows:

$$0 = \sum_{j=1}^{J-1} \frac{2m}{\hbar^2} \mathrm{Im}\,(z)|u_j|^2 - \frac{\mathrm{Im}\,(\beta_2(z))}{\Delta x^2}|u_J|^2 - \frac{\mathrm{Im}\,(\alpha_2(z))}{\Delta x^2}|u_0|^2$$

Using $u^H u = 1$ and (B.11), the previous equation implies $\mathrm{Im}\,(z) < 0$. ∎

C Resolution of the time-dependent Schrödinger equation

Although in the applications considered here the potential depends nonlinearly on the wave function, this section is written in the case of the linear Schrödinger equation. As in [17] and [43], the extension to the nonlinear case is provided by an adapted choice of the potential at half time step.

C.1 The homogeneous case

In this section, we recall the scheme proposed in [18] to solve on the bounded domain $[0, L]$ the time-dependent Schrödinger equation

$$\begin{cases} i\hbar\partial_t \Psi = -\frac{\hbar^2}{2m}\partial_x^2 \Psi + Q\Psi, & t > 0,\, x \in I\!R \\ \Psi(0,x) = \Phi(x), & x \in I\!R\,, \end{cases} \tag{C.1}$$

with the following hypothesis:

*H*1. The initial condition Φ is supported in $0 < x < L$.

*H*2. The potential Q verifies: for $t > 0$

$$Q(t,x) = 0,\, x \le 0, \quad \text{and} \quad Q(t,x) = Q_L,\, x \ge L\,.$$

Considering the time and space discretization defined in section 4.1, we note $Q_j^{l+1/2}$ the approximation of the potential $Q(t^{l+1/2}, x_j)$ and Ψ_j^l the approximation of the solution $\Psi(t^l, x_j)$. Then, equation (C.1), is solved with the Crank-Nicolson method:

$$i\hbar D_t^+ \Psi_j^l = -\frac{\hbar^2}{2m} D_x^2 \Psi_j^{l+1/2} + Q_j^{l+1/2}\Psi_j^{l+1/2}, \quad j = 1, ..., J-1, \quad l \ge 0, \tag{C.2}$$

where

$$D_t^+ \Psi_j^l = \frac{\Psi_j^{l+1} - \Psi_j^l}{\Delta t} \quad \text{and} \quad \Psi_j^{l+1/2} = \frac{1}{2}\left(\Psi_j^l + \Psi_j^{l+1}\right) \tag{C.3}$$

The equation (C.2) comes with the discrete transparent boundary conditions:

$$\Psi_1^l - s_0^0 \Psi_0^l = \sum_{k=1}^{l-1} s_0^{l-k}\Psi_0^k - \Psi_1^{l-1}, \quad l \ge 1, \tag{C.4}$$

$$\Psi_{J-1}^l - s_J^0 \Psi_J^l = \sum_{k=1}^{l-1} s_J^{l-k}\Psi_J^k - \Psi_{J-1}^{l-1}, \quad l \ge 1, \tag{C.5}$$

where, we have for $j = 0$ and $j = J$:

$$s_j^l = \left[1 - i\frac{R}{2} + \frac{\sigma_j}{2}\right]\delta_l^0 + \left[1 + i\frac{R}{2} + \frac{\sigma_j}{2}\right]\delta_l^1 + \alpha_j \exp\left(-il\varphi_j\right)\frac{P_l(\mu_j) - P_{l-2}(\mu_j)}{2l-1}, \tag{C.6}$$

and

$$\varphi_j = \arctan \frac{2R(\sigma_j+2)}{R^2-4\sigma_j-\sigma_j^2}, \quad \mu_j = \frac{R^2+4\sigma_j+\sigma_j^2}{\sqrt{(R^2+\sigma_j^2)[R^2+(\sigma_j+4)^2]}}$$

$$\sigma_j = \frac{2m\Delta x^2}{\hbar^2}Q_j, \quad \alpha_j = \frac{i}{2}((R^2+\sigma_j^2)[R^2+(\sigma_j+4)^2])^{1/4}\exp\left(i\frac{\varphi_j}{2}\right), \quad R = \frac{4m\Delta x^2}{\hbar\Delta t}\,.$$

Here P_l denotes the Legendre polynomials with the convention $P_{-1} = P_{-2} = 0$, δ_l^j the Kronecker symbol related to the integers j, l and $Q_0 = 0$, $Q_J = Q_L$. The coefficients s_j^l are computed thanks to the recurrence formula derived in [18] from the standard recursion formula for the Legendre polynomials.
We remark that the scheme (C.2) with the boundary conditions (C.4)(C.5) has a unique solution. By construction, the unique $L^2(\mathbb{Z})$-solution Ψ_j^l to the whole-space scheme (C.2) considered on $j \in \mathbb{Z}$ verifies the problem (C.2)(C.4)(C.5). It follows that the solution to (C.2)(C.4)(C.5) corresponds exactly with the restriction of Ψ_j^l to $0 \le j \le J$. Moreover, we have the following stability result:

Theorem C.1 ([18]). *The solution to the discrete Schrödinger equation* (C.2) *with the boundary conditions* (C.4)(C.5) *is uniformly bounded:*

$$\|\Psi^l\|_2 \le \|\Psi^0\|_2, \quad l \ge 1$$

and therefore, the scheme is unconditionally stable.

C.2 The non-homogeneous case

C.2.1 The non-homogeneous discrete transparent boundary conditions

We consider the problem (C.1) where the initial condition Φ is solution to (A.2). We make the assumption that the potentials Q_I and Q are such that (A.1) and $H2$ hold and $Q(0,x) = Q_I(x)$. Like in section C.1, we will use the Crank-Nicolson scheme (C.2), however, the hypothesis $H1$ is not verified and we can not apply (C.4)(C.5).
Nevertheless, using equations (C.1) and (A.2), the function

$$\varphi = \Psi - \Phi e^{-i\omega_0 t}\,, \tag{C.7}$$

where

$$\omega_0 = \frac{E_I}{\hbar}\,, \tag{C.8}$$

is solution to:

$$i\hbar\partial_t\varphi = [-\frac{\hbar^2}{2m}\partial_x^2 + Q]\varphi, \quad x \le 0$$

and verifies $\varphi(0,x) = 0$. Thus, we can write the homogeneous boundary condition (C.4) for φ which gives the following boundary condition at $x = 0$ for Ψ:

$$\Psi_1^l - s_0^0\Psi_0^l = \sum_{k=1}^{l-1} s_0^{l-k}\left(\Psi_0^k - \Phi_0 e^{-i\omega_0 t^k}\right) - \left(\Psi_1^{l-1} - \Phi_1 e^{-i\omega_0 t^{l-1}}\right) + \Phi_1 e^{-i\omega_0 t^l} - s_0^0\Phi_0 e^{-i\omega_0 t^l}, \quad l \ge 1 \tag{C.9}$$

where the coefficients s_j^l are given by (C.6) and Φ_j is provided by the resolution to the stationary discrete problem (A.3). We proceed similarly at $x = L$ by setting

$$\varphi = \Psi - \Phi e^{-i\omega_L t} \tag{C.10}$$

where

$$\omega_L = \frac{1}{\hbar}(E_I + Q_L - Q_{I,L})\,. \tag{C.11}$$

We obtain the following boundary condition at $x = L$:

$$\Psi^l_{J-1} - s^0_J \Psi^l_J = \sum_{k=1}^{l-1} s^{l-k}_J \left(\Psi^k_J - \Phi_J e^{-i\omega_L t^k} \right) - \left(\Psi^{l-1}_{J-1} - \Phi_{J-1} e^{-i\omega_L t^{l-1}} \right) + \Phi_{J-1} e^{-i\omega_L t^l} - s^0_J \Phi_J e^{-i\omega_L t^l}, \quad l \geq 1 . \quad \text{(C.12)}$$

C.2.2 Discrete angular frequencies, stability

Since the homogeneous transparent boundary conditions (C.4)(C.5) are derived from the fully discrete scheme (C.2) where $j \in \mathbb{Z}$, the accuracy of the non-homogeneous boundary conditions (C.9)(C.12) is improved under the condition that the functions in (C.7) and (C.10) are solutions to the discrete equation (C.2) for $j \leq 0$ and respectively $j \geq J$. As shown in [3], this leads to the non-homogeneous boundary conditions (C.9)(C.12) we obtained here, where the angular frequencies given in (C.8) and (C.11) have to be replaced by the discrete ones below:

$$\omega_0 = \frac{2}{\Delta t} \arctan \left(\frac{\Delta t E_I}{2\hbar} \right) \quad \text{(C.13)}$$

$$\omega_L = \frac{2}{\Delta t} \arctan \left(\frac{\Delta t}{2\hbar} (E_I + Q_L - Q_{I,L}) \right) \quad \text{(C.14)}$$

We remark that, for $k > 0$, the solution to the initial finite difference scheme (A.3) considered on $j \in \mathbb{Z}$ with the scattering conditions (A.6)(A.9) is in $L^\infty(\mathbb{Z})$ but not in $L^2(\mathbb{Z})$. The same property is true for $k < 0$. Therefore, for such an initial condition, the whole-space scheme (C.2) considered on $j \in \mathbb{Z}$ has a unique solution $\Psi^l_j \in L^2(\mathbb{Z}) + L^\infty(\mathbb{Z})$. By construction, Ψ^l_j verifies the problem (C.2) with the boundary conditions (C.9)(C.12) where the angular frequencies are given by (C.13)(C.14). It follows that the unique solution to (C.2)(C.9)(C.12) corresponds exactly with the restriction of Ψ^l_j to $0 \leq j \leq J$. Moreover, we have the following nice stability result:

Theorem C.2. *Let Φ be the solution to the scheme* (A.3) *with the boundary conditions* (A.7)(A.10) *for $k > 0$ and* (A.11)(A.12) *for $k < 0$. Let Ψ be the solution to the discrete Schrödinger equation* (C.2) *with the non-homogeneous boundary conditions* (C.9)(C.12) *and the initial condition $\Psi^0 = \Phi$. We suppose in addition that the angular frequencies ω_0 and ω_L in* (C.9)(C.12) *are given by* (C.13)(C.14). *Then, there exists a constant $C > 0$ which depends only on $\hbar$, m, L, $Q_{I,L}$, $\sup_{x\in(0,L)} |Q_I(x)|$, Q_L, k such that for all Δx verifying* (A.4) *it holds for all $N \geq 0$:*

$$\|\Psi^l\|_2 \leq C \left[\left(1 + \max_{0\leq n\leq N} \|Q^{n+1/2}\|_\infty \right) T + 1 \right], \quad 0 \leq l \leq N$$

where $T = N\Delta t$ and $\|Q^{n+1/2}\|_\infty = \max_{1\leq j\leq J-1} |Q^{n+1/2}_j|$.

Even if no size limit on the time step is deduced from Theorem C.2, the time oscillating terms $e^{-i\omega_0 t}$ and $e^{-i\omega_L t}$ in (C.9) and respectively (C.12) require the following condition for a suitable resolution:

$$|\omega_j| \Delta t < \frac{\pi}{2}, \quad j = 0, L \quad \text{(C.15)}$$

We can now give the proof of Theorem C.2:

Proof. We can suppose without any practical restriction that $J \geq 3$. Then, consider a smooth function χ such that

$$0 \leq \chi(x) \leq 1, \ x \in I\!R, \quad \chi(x) = 1, \ x \leq \frac{L}{3}, \quad \chi(x) = 0, \ x \geq \frac{2L}{3}$$

Using the vector $\chi_j = \chi(x_j)$, we define for $l \geq 0$ and $0 \leq j \leq J$:

$$\theta^l_j = \chi_j \Phi_j e^{-i\omega_0 t^l} + (1 - \chi_j) \Phi_j e^{-i\omega_L t^l}$$

and

$$\varphi_j^l = \Psi_j^l - \theta_j^l$$

Using the scheme (C.2) for Ψ, we obtain the discrete Schrödinger equation below for the function φ:

$$i\hbar D_t^+ \varphi_j^l = -\frac{\hbar^2}{2m} D_x^2 \varphi_j^{l+1/2} + Q_j^{l+1/2} \varphi_j^{l+1/2} + F_j^l, \quad j = 1, ..., J-1, \quad l \geq 0 \tag{C.16}$$

with source term

$$F_j^l = -i\hbar D_t^+ \theta_j^l - \frac{\hbar^2}{2m} D_x^2 \theta_j^{l+1/2} + Q_j^{l+1/2} \theta_j^{l+1/2}$$

where $\varphi_j^{l+1/2}$, $\theta_j^{l+1/2}$ are defined as in (C.3). Multiplying equation (C.16) by $\overline{\varphi}_j^{l+1/2}$ and summing up for $j = 1, ..., J-1$, it follows:

$$\begin{aligned} i\hbar \sum_{j=1}^{J-1} D_t^+ \varphi_j^l \overline{\varphi}_j^{l+1/2} = \frac{\hbar^2}{2m} \sum_{j=0}^{J-1} \left| D_x^+ \varphi_j^{l+1/2} \right|^2 + \sum_{j=1}^{J-1} Q_j^{l+1/2} \left| \varphi_j^{l+1/2} \right|^2 \\ - \frac{\hbar^2}{2m\Delta x} \left(D_x^+ \varphi_{J-1}^{l+1/2} \overline{\varphi}_J^{l+1/2} - D_x^+ \varphi_0^{l+1/2} \overline{\varphi}_0^{l+1/2} \right) + \sum_{j=1}^{J-1} F_j^l \overline{\varphi}_j^{l+1/2} \end{aligned}$$

where we used the summation by part rule (B.12). Taking the imaginary part, we get:

$$D_t^+ \|\varphi^l\|_2^2 = \frac{\hbar}{m} \left[-\mathrm{Im} \left(D_x^- \varphi_J^{l+1/2} \overline{\varphi}_J^{l+1/2} \right) + \mathrm{Im} \left(D_x^+ \varphi_0^{l+1/2} \overline{\varphi}_0^{l+1/2} \right) \right] + \frac{2\Delta x}{\hbar} \sum_{j=1}^{J-1} \mathrm{Im} \left(F_j^l \overline{\varphi}_j^{l+1/2} \right)$$

The initial condition $\varphi^0 = 0$ obviously holds, therefore we have by summing up with respect to l in the previous equation:

$$\begin{aligned} \|\varphi^{N+1}\|_2^2 = \frac{\hbar \Delta t}{m} \left[-\mathrm{Im} \left(\sum_{l=0}^{N} D_x^- \varphi_J^{l+1/2} \overline{\varphi}_J^{l+1/2} \right) + \mathrm{Im} \left(\sum_{l=0}^{N} D_x^+ \varphi_0^{l+1/2} \overline{\varphi}_0^{l+1/2} \right) \right] \\ + \frac{2\Delta x \Delta t}{\hbar} \sum_{l=0}^{N} \sum_{j=1}^{J-1} \mathrm{Im} \left(F_j^l \overline{\varphi}_j^{l+1/2} \right) \end{aligned} \tag{C.17}$$

for all $N \geq 0$. Since the non-homogeneous boundary conditions (C.9)(C.12) hold for Ψ, it follows that the homogeneous ones (C.4)(C.5) hold for φ. Therefore, the boundary terms in (C.17) behave like in Theorem C.1. In particular, it is shown in [18] that the boundary conditions (C.4)(C.5) imply:

$$-\mathrm{Im} \left(\sum_{l=0}^{N} D_x^- \varphi_J^{l+1/2} \overline{\varphi}_J^{l+1/2} \right) \leq 0, \quad \mathrm{Im} \left(\sum_{l=0}^{N} D_x^+ \varphi_0^{l+1/2} \overline{\varphi}_0^{l+1/2} \right) \leq 0$$

Then, it follows from (C.17) that:

$$\|\varphi^{N+1}\|_2^2 \leq \frac{2\Delta t}{\hbar} \sum_{l=0}^{N} \left\| F^l \right\|_2 \left\| \varphi^{l+1/2} \right\|_2 \tag{C.18}$$

Using the equations (C.13)(C.14) and the equation (A.3), with the boundary conditions (A.7)(A.10) for $k > 0$ and (A.11)(A.12) for $k < 0$, and using the result of Lemma A.1, the following estimates holds for the source term:

$$\left\| F^l \right\|_2 \leq C \left(1 + \max_{0 \leq n \leq N} \|Q^{n+1/2}\|_\infty \right), \quad 0 \leq l \leq N \tag{C.19}$$

where C denotes a constant which depends only on $\hbar$, m, L, $Q_{I,L}$, $\sup_{x \in (0,L)} |Q_I(x)|$, Q_L, k. After some manipulations, the inequalities (C.18) and (C.19) lead to:

$$\left\| \varphi^l \right\|_2 \leq C \left(1 + \max_{0 \leq n \leq N} \|Q^{n+1/2}\|_\infty \right) T, \quad 0 \leq l \leq N \tag{C.20}$$

where $T = N\Delta t$. Applying (C.20) and Lemma A.1 again, the inequality

$$\left\|\Psi^l\right\|_2 \leq \left\|\varphi^l\right\|_2 + \left\|\theta^l\right\|_2 \leq \left\|\varphi^l\right\|_2 + 2\left\|\Phi\right\|_2$$

achieves the proof. ■

C.2.3 Simplified discrete transparent boundary conditions

As proposed in [18], the computational time can be reduced using the decay of the coefficients s_j^n appearing in (C.9)(C.12). This improvement is obtained by replacing the coefficients s_j^n by 0 after an index $M \geq 1$ chosen big enough to preserve the accuracy of the boundary conditions. In that case, the numerical cost of the convolutions in (C.9)(C.12) is reduced and the computations are performed as follows: for $1 \leq l \leq M+1$ the boundary conditions are given by (C.9)(C.12) and for $l \geq M+2$, they are given by:

$$\Psi_1^l - s_0^0\Psi_0^l = \sum_{k=l-M}^{l-1} s_0^{l-k}\left(\Psi_0^k - \Phi_0 e^{-i\omega_0 t^k}\right) - \left(\Psi_1^{l-1} - \Phi_1 e^{-i\omega_0 t^{l-1}}\right) + \Phi_1 e^{-i\omega_0 t^l} - s_0^0\Phi_0 e^{-i\omega_0 t^l} \tag{C.21}$$

and

$$\Psi_{J-1}^l - s_J^0\Psi_J^l = \sum_{k=l-M}^{l-1} s_J^{l-k}\left(\Psi_J^k - \Phi_J e^{-i\omega_L t^k}\right) - \left(\Psi_{J-1}^{l-1} - \Phi_{J-1} e^{-i\omega_L t^{l-1}}\right) + \Phi_{J-1} e^{-i\omega_L t^l} - s_J^0\Phi_J e^{-i\omega_L t^l} \tag{C.22}$$

References

[1] J. Aguilar, J. M. Combes, A Class of Analytic Perturbations for One-body Schrödinger Hamiltonians, Commun. math. Phys. 22, 4 (1971) 269-279.

[2] X. Antoine, C. Besse, Construction, structure and asymptotic approximations of a microdifferential transparent boundary condition for the linear Schrdinger equation, J. Math. Pures Appl. 80, 7 (2001) 701-738.

[3] A. Arnold, Mathematical concepts of open quantum boundary conditions, Transp. Theory Stat. Phys. 30, 4-6 (2001) 561-584.

[4] W. Z. Bao, S. Jin, P. A. Markowich, Numerical Study of Time-Splitting Spectral Discretizations of Nonlinear Schrödinger Equations in the Semiclassical Regimes, SIAM J. Sci. Comput. 25, 1 (2003) 27-64.

[5] N. Ben Abdallah, M. Mouis, C. Negulescu, An accelerated algorithm for 2D simulations of the quantum ballistic transport in nanoscale MOSFETs, J. Comput. Phys. 225, 1 (2007) 74-99.

[6] N. Ben Abdallah, P. Degond, P. A. Markowich, On a one-dimensional Schrödinger-Poisson scattering model, Z. angew. Math. Phys. 48, 1 (1997) 135-155.

[7] N. Ben Abdallah, O. Pinaud, A mathematical model for the transient evolution of a resonant tunneling diode, C. R. Acad. Sci. Paris, Ser. I 334, 4 (2002) 283-288.

[8] N. Ben Abdallah, O. Pinaud, Multiscale simulation of transport in an open quantum system: Resonances and WKB interpolation, J. Comput. Phys. 213, 1 (2006) 288-310.

[9] N. Ben Abdallah, H. Wu, A Generalized Stationary Algorithm for Resonant Tunneling: Multi-Mode Approximation and High Dimension, Commun. Comput. Phys. 10, 4 (2011) 882-898.

[10] C. Besse, A Relaxation Scheme for the Nonlinear Schrödinger Equation, SIAM J. Numer. Anal. 42, 3 (2004) 934-952.

[11] D. Bindel, M. Zworski, Symmetry of Bound and Antibound States in the Semiclassical Limit, Lett. Math. Phys. 81, 2 (2007) 107-117.

[12] V. Bonnaillie-Noël, A. Faraj, F. Nier, Simulation of resonant tunneling heterostructures: numerical comparison of a complete Schrödinger-Poisson system and a reduced nonlinear model, J. Comput. Electron. 8, 1 (2009) 11-18.

[13] V. Bonnaillie-Noël, F. Nier, Y. Patel, Computing the steady states for an asymptotic model of quantum transport in resonant heterostructures, J. Comput. Phys. 219, 2 (2006) 644-670.

[14] V. Bonnaillie-Noël, F. Nier, Y. Patel, Far from equilibrium steady states of 1D-Schrödinger-Poisson systems with quantum wells I, Ann. I. H. Poincaré-AN 25, 5 (2008) 937-968.

[15] V. Bonnaillie-Noël, F. Nier, Y. Patel, Far from equilibrium steady states of 1D-Schrödinger-Poisson systems with quantum wells II, J. Math. Soc. Japan 61, 1 (2009) 65-106.

[16] F. Brezzi, P. A. Markowich, The three-dimensional Wigner-Poisson problem: Existence, uniqueness and approximation, Math. Meth. App. Sci. 14, 1 (1991) 35-61.

[17] Q. Chang, E. Jia, W. Sun, Difference Schemes for Solving the Generalized Nonlinear Schrödinger Equation, J. Comput. Phys. 148, 2 (1999) 397-415.

[18] M. Ehrhardt, A. Arnold, Discrete Transparent Boundary Conditions for the Schrödinger Equation, Rivista di Matematica della Universita di Parma 6, 4 (2001) 57-108.

[19] A. Faraj, Méthodes asymptotiques et numériques pour le transport quantique résonnant, Thèse de doctorat, Université de Toulouse, 2008.

[20] A. Faraj, A. Mantile, F. Nier, Adiabatic evolution of 1D shape resonances: an artificial interface conditions approach, Math. Model. Meth. Appl. Sci. 21, 3 (2011) 541-618.

[21] A. Faraj, A. Mantile, F. Nier, An explicit model for the adiabatic evolution of quantum observables driven by 1D shape resonances, J. Phys. A: Math. Theor. 43 (2010) 474025.

[22] W. R. Frensley, Boundary conditions for open quantum systems driven far from equilibrium, Rev. Mod. Phys. 62, 3 (1990) 745-791.

[23] S. Fujiié, T. Ramond, Matrice de scattering et résonances associées à une orbite hétérocline, Ann. Inst. Henri Poincaré (A) 69, 1 (1998) 31-82.

[24] C. Greengard, P. A. Raviart, A boundary-value problem for the stationary Vlasov-Poisson equations: The plane diode, Comm. Pure Appl. Math. 43, 4 (1990) 473-507.

[25] P. Guillaume, Nonlinear Eigenproblems, SIAM J. Matrix Anal. Appl. 20, 3 (1999) 575-595.

[26] H. K. Gummel, A self-consistent iterative scheme for one-dimensional steady state transistor calculations, IEEE Trans. Elec. Dev. 11, 10 (1964) 455-465.

[27] P. D. Hislop, I. M. Sigal, Introduction to Spectral Theory with Applications to Schrödinger Operators, Applied Mathematical Sciences 113, Springer-Verlag, New York, 1996.

[28] S. Jin, H. Wu, X. Yang, The Gaussian Beam Methods for Schrödinger-Poisson Equations, J. Comp. Math. 28, 2 (2010) 261-272.

[29] G. Jona-Lasinio, C. Presilla, J. Sjöstrand, On Schrödinger Equations with Concentrated Nonlinearities, Ann. Phys. 240, 1 (1995) 1-21.

[30] L. V. Iogansen, The possibility of resonance transmission of electrons in crystals through a system of barriers, Soviet Physics JETP 18 (1964) 146.

[31] C. S. Lent, D. J. Kirkner, The quantum transmitting boundary method, J. Appl. Phys. 67, 10 (1990) 6353-6359.

[32] P. L. Lions, T. Paul, Sur les mesures de Wigner, Rev. Mat. Iberoam. 9, 3 (1993) 553-618.

[33] H. Mizuta, T. Tanoue, The Physics and Applications of Resonant Tunnelling Diodes, Cambridge University Press, Cambridge, 1995.

[34] C. Negulescu, Numerical analysis of a multiscale finite element scheme for the resolution of the stationary Schrödinger equation, Numer. Math. 108, 4 (2008) 625-652.

[35] F. Nier, The dynamics of some quantum open systems with short-range nonlinearities, Nonlinearity 11, 4 (1998) 1127-1172.

[36] Y. Patel, Développement de modèles macroscopiques pour des systèmes quantiques nonlinéaires hors-équilibre, Thèse de doctorat, Université de Rennes 1, 2005.

[37] G. Peters, J. H. Wilkinson, Inverse Iteration, Ill-Conditioned Equations and Newton's Method, SIAM Rev. 21, 3 (1979) 339-360.

[38] O. Pinaud, Transient simulations of a resonant tunneling diode, J. App. Phys. 92, 4 (2002) 1987-1994.

[39] F. Poupaud, Boundary value problems for the stationary Vlasov-Maxwell system, Forum Math. 4 (1992) 499-527.

[40] C. Presilla, J. Sjöstrand, Transport properties in resonant tunneling heterostructures, J. Math. Phys. 37, 10 (1996) 4816-4844.

[41] U. V. Riss, H. D. Meyer, Calculation of resonance energies and widths using the complex absorbing potential method, J. Phys. B: At. Mol. Opt. Phys. 26 (1993) 4503-4536.

[42] R. Tsu, L. Esaki, Tunneling in a finite superlattice, Appl. Phys. Lett. 22, 11 (1973) 562-564.

[43] A. Zisowsky, M. Ehrhardt, Discrete artificial boundary conditions for nonlinear Schrödinger equations, Math. Comput. Model. 47, 11-12 (2008) 1264-1283.